The Ferrous Iron Transporter FeoB1 is Essential for *Clostridioides difficile* Toxin Production and Pathogenesis in Mice

Aditi Deshpande[1], Abiola O. Olaitan[1, +], Ann M. Mckelvey[1, +], Jacob T. Rutherford[1], Julian G. Hurdle[1]*

[1]Center for Infectious and Inflammatory Diseases, Institute of Biosciences and Technology, Texas A&M Health Science Center, 2121 West Holcombe Blvd, Houston, Texas 77030, USA

*Correspondence and requests for materials should be addressed to J.G.H (jhurdle@tamu.edu).

[+]Both authors equally contributed to this work.

Running title: Loss of *feoB1* attenuates *C. difficile* virulence

Keywords: pyruvate metabolism, iron limitation, avirulence, infectious colitis

ABSTRACT

Ferrous iron is the dominant form of iron in the oxygen-limited large intestine, the site for *Clostridioides difficile* infection (CDI). We investigated the extent to which *C. difficile* requires the ferrous iron transporter 1 (FeoB1), a main permease for iron acquisition, using *in vitro* and *in vivo* approaches. Construction of *feoB1* deletion mutant in *C. difficile* R20291 (i.e., R20291Δ*feoB1*) decreased intracellular iron content by ~25%. This was accompanied by reduced synthesis of TcdA and TcdB toxins and downregulation of *tcdA* and *tcdB* genes, which was reflected by a ~1000-fold reduction in cytopathy against Vero cells. Complementation with WT *feoB1* restored toxin production. R20291Δ*feoB1* was avirulent in mice with underlying colitis. In this model, mice are prone to develop severe CDI, but mice infected with the mutant lacked diarrheal symptoms, had lesser inflammatory responses, bacterial bioburdens and cecal toxin titers. Transcriptional and biochemical analyses revealed Δ*feoB1* altered metabolic pathways that negatively impact toxin production, including downregulation of the oxidative branch of the Kreb cycle and an associated cellular accumulation of pyruvate. Hence FeoB1 influences multiple bioenergetic and redox pathways, which in turn inhibits toxin biosynthesis. Targeting FeoB1 could be a potential therapeutic strategy to impede the colonization and pathogenesis of *C. difficile*, even in the setting of colitis where CDI is more severe and intestinal bleeding may occur.

AUTHOR SUMMARY

Clostridioides difficile is a major cause of antibiotic associated diarrhea that result in significant morbidity and mortality in hospitals. The ability of *C. difficile* to cause disease and damage the gut is directly related to the production of toxin A and toxin B. Without these toxins, *C. difficile* is not virulent. There is need to identify drug targets and therapeutic strategies that prevent *C. difficile* from producing toxins A and B. For *C. difficile* to colonize the large bowel, it must acquire ferrous iron, which is thought to be the main form of iron within the oxygen-limited large bowel environment. We show that genetic deletion of the ferrous iron transporter FeoB1 stops *C. difficile* from producing significant amounts of toxins under *in vitro* conditions. Importantly, the mutant R20291Δ*feoB1* was avirulent when tested in a mouse model that favors the development of severe infections. Avirulence of R20291Δ*feoB1* was related to the strain having significant metabolic changes that negatively impact toxin production. For example, cells could not properly metabolize pyruvate, which became accumulated in cells; pyruvate is known to reduce the production of toxins A and B. Our study provides new insights into how FeoB1 affects *C. difficile* colonization and disease development, indicating FeoB1 could be a drug target to stop toxin production in this bacterium.

58 **INTRODUCTION**

59

60 *Clostridioides difficile* infection (CDI) is a leading cause of hospital-acquired diarrhea, with
61 30,600 and 20,500 in-hospital deaths in 2011 and 2017, respectively [1]. The main risk factor for
62 CDI is prior antibiotic use, which causes dysbiosis [2]. Treatment with anti-*C. difficile* antibiotics,
63 vancomycin, metronidazole or fidaxomicin, are associated with recurrence rates that may be ≥10%
64 or higher [3-5]. Understanding the pathophysiology of *C. difficile* provides a basis to discover
65 alternative therapeutics to prevent or treat recurrent disease.

66

67 CDI symptoms range from mild-to-moderate diarrhea to severe pseudomembranous colitis,
68 resulting from epithelial damage by *C. difficile* toxins TcdA and TcdB [6]. These toxins
69 glycosylate GTPases (e.g., Rho, Rac, Cdc42) to block actin polymerization, causing cells to appear
70 rounded in tissue cultures [6]. Genes (*tcdA* and *tcdB*) encoding TcdA and TcdB are chromosomally
71 located in the pathogenicity locus (PaLoc) [6]. PaLoc encodes the alternative sigma factor TcdR,
72 which activates transcription of *tcdA* and *tcdB*; the TcdR antagonist TcdC that represses *tcdA* and
73 *tcdB*; and the holin-like protein TcdE that exports the toxins. TcdA and TcdB are produced in the
74 late logarithmic and stationary phases of growth and are regulated by environmental and nutritional
75 changes. For example, *tcdA* and *tcdB* are repressed by metabolizable sugars (e.g., glucose) and
76 metabolism of amino acids like proline, cysteine, and branched-chain amino acids (BCAAs) [7-
77 9]. Glucose activates catabolite repression whereby the global regulator CcpA binds upstream of
78 promoters in PaLoc, particularly the *tcdR* promoter, to block transcription of *tcdA* and *tcdB* [7].
79 During logarithmic growth, high intracellular concentrations of GTP bind to the nutritional
80 regulator CodY, which in turn binds to regions of the *tcdR* promoter [10]. Through an unclear
81 mechanism, pyruvate represses transcription of *tcdA* and *tcdB* [9]. Conversely, butyrate enhances

82 the synthesis of toxins by an unknown mechanism that may be related to NAD+ regeneration via
83 alternative fermentative pathways that produce butyrate [11]. These and other examples, reviewed
84 by Martin-Verstraete et al. [12] and Bouillaut et al. [13], all point to there being a complex
85 metabolic and regulatory network for *C. difficile* toxin production.
86
87 Within environments that are anaerobic and acidic, such as the gastrointestinal tract, iron mainly
88 exists as ferrous iron [14]. Gut bacteria must therefore be able to obtain ferrous iron in the
89 microaerophilic and anaerobic niches of the intestine. The high affinity ferrous iron transporter
90 (Feo transporter) plays an essential role in iron acquisition by bacteria in the intestinal tract [14,
91 15]. The Feo transporter mainly consists of FeoA, a small cytoplasmic protein, and FeoB, the
92 membrane-bound permease that transports ferrous iron into cells. While the specific role of FeoA
93 is still unclear, it might interact with the cytoplasmic domain of FeoB to regulate ferrous iron
94 transport. Iron is indispensable for *C. difficile* growth and pathogenesis [16, 17] as several essential
95 redox-associated proteins require the iron containing cofactor ferredoxin (Fdx) or iron-sulfur
96 clusters. *C. difficile* possesses three homologs of the FeoB permease, designated FeoB1, FeoB2
97 and FeoB3 [17]. Under iron-limiting conditions, *feoB1* is the most transcribed *feo* homolog [9, 16,
98 17]; hence, FeoB1 is thought to be the main permease for ferrous iron acquisition in *C. difficile*.
99 However, it is unknown whether FeoB1-mediated iron acquisition is critical for production of
100 TcdA and TcdB.
101
102 *Clostridium perfringens* encodes a single FeoB transporter, and its deletion reduced growth and
103 impaired iron-dependent fermentation and expression of the virulence toxins phospholipase C and
104 perfringolysin O [18]. However, the authors [18] reasoned that reduced toxin production in *C.*

105 *perfringens* resulted from the effects on growth. Conversely, in *C. difficile*, deletion of *feoB1* in
106 non-toxigenic ATCC 700057 did not affect growth in Brain Heart Infusion (BHI) broth, but
107 reduced iron content [19]. This is particularly interesting since iron deficiency in *C. difficile*
108 disturbs several metabolic processes, including shifting cells from ferredoxin to flavodoxin-
109 mediated metabolism; increasing intracellular concentrations of pyruvate and glucose [16, 19]; and
110 enhancing proline reduction via Stickland metabolism [16]. We therefore investigated whether
111 iron deficiency caused by loss of *feoB1* impacts *C. difficile* toxin production and pathogenesis.
112 Herein, we show that deletion of *feoB1* markedly abolishes toxin production and pathogenesis of
113 *C. difficile* in mice.
114
115 **RESULTS AND DISCUSSION**
116
117 **Loss of *feoB1* impairs toxin production.** R20291 was adopted as a model strain of epidemic
118 ribotype 027 [20] to delete *feoB1* by allelic exchange to generate R20291Δ*feoB1*; deletion was
119 confirmed by PCR and Sanger sequencing (**Fig S1**). Growth of R20291Δ*feoB1* in BHI broth was
120 not substantially affected, when compared to WT R20291 (**Fig 1A**); BHI broth contained 0.5 ppm
121 of iron. Measurement of intracellular iron content, by ICP-OES, revealed there was a ~25%
122 reduction in iron content in R20291Δ*feoB1* (0.087 ± 0.006 ppm) compared to the WT (0.116 ±
123 0.007 ppm) (**Fig 1B**; $p \leq 0.01$, by unpaired t-test). These results are comparable to *feoB1* deletion
124 mutant of non-toxigenic ATCC 700057, which had a ~21% reduction in iron content without
125 attenuated growth in BHI broth [19]. We next quantified toxins in the supernatants of 24 h cultures
126 using an ELISA kit from tgcBIOMICS GmbH. Toxin concentrations in R20291Δ*feoB1* for TcdA
127 (5.37 ± 0.66 ng/ml) and TcdB (3.51 ± 0.48 ng/ml) were significantly lower ($p<0.0001$ and $p<0.001$,
128 by unpaired t-test) than those produced by WT R20291 (19.65 ± 0.67 ng/ml; and 11.46 ± 0.69
129 ng/ml, respectively) (**Fig 1C**). Complementation of R20291Δ*feoB1* with WT *feoB1*, ectopically

130 expressed from its own promoter, increased the synthesis of both toxins (10.42 ± 0.66 ng/ml; and
131 6.77 ± 0.18 ng/ml, for TcdA and TcdB, respectively (**Fig 1C**). Comparable results were attained
132 in cytopathic assays that measure toxin-induced cell rounding of mammalian cells and detects
133 picomolar amounts of toxins [21]. Against Vero cells, R20291Δ*feoB1* had toxin titers of $\leq 10^1$,
134 which was 1000-fold lower than the titers of WT cultures (10^4 toxin titer; **Fig. 1D**); the
135 complemented strain (R20291Δ*feoB1*_WT *feoB1*) had toxin titers of 10^3 to 10^4. These findings
136 were confirmed by automated morphometric analysis of cell rounding to avoid potential bias from
137 manual visualization of cells (**Fig 1E**); the in-situ dilution of supernatants was ~1:1000 and
138 rounding of Vero cells is more due to TcdB as it is more refractory to TcdA [22]. WT R20291,
139 R20291Δ*feo*B1 and R20291Δ*feoB1*_WT *feoB1* caused 88.70 ± 1.60, 10.54 ± 0.52 and 52.02 ± 0.74
140 percentage cell rounding for three replicates, respectively. Taken together, Δ*feoB1* diminished
141 intracellular iron content and restricted the biosynthesis of TcdA and TcdB, without affecting
142 growth rates in R20291.
143
144 **Deletion of *feoB1* attenuated virulence in mice with colitis CDI.** *In vivo* pathogenesis of
145 R20291Δ*feoB1* was investigated in a reported murine model of colitis CDI [23] that we modified
146 by using a lower concentration of dextran sodium sulfate (DSS; 1.5% w/v instead of 3% w/v) and
147 administering antibiotics and DSS for 5 days, as oppose to 3 days (**Fig 2A**). These modifications
148 reduced reported DSS-related morbidity and deaths [23]. Because this model is characterized by
149 intestinal bleeding [23] it enabled assessment of R20291Δ*feoB1* virulence in a setting that favors
150 iron availability at the site of infection. We performed two independent experiments. Ceca from
151 animals infected with R20291 were inflamed, whereas ceca from animals infected with
152 R20291Δ*feoB1* were like those from uninfected mice (**Fig 2B**). Infection with WT R20291 was
153 lethal to C57BL/6 mice as half of sixteen mice survived. In contrast, all fifteen mice survived that

154 were infected with R20291Δ*feoB1* (**Fig 2C**); p=0.0003 according to log rank test. Significant
155 weight loss was only observed in animals infected with R20291 and is a common symptom of
156 acute CDI in mice (**Fig 2D**); however, mice infected with R20291Δ*feoB1* either gained weight or
157 experienced marginal weight loss (p=0.0009 according to unpaired t-test). Animals that
158 succumbed to infection with R20291 had endpoint spore bioburdens of ~10^7 CFU/ml that were
159 significantly higher than bioburdens from animals that survived infection (i.e., ~2 logs [~99%]
160 greater; p<0.0001 determined by unpaired t-test; **Fig 2E**). Animals infected with R20291Δ*feoB1*
161 had even lower bioburdens than the surviving animals infected with the WT R20291 (i.e., >1 log
162 [~93%] higher; p<0.0001 determined by unpaired t-test; **Fig 2E**). As a quality control, cecal
163 isolates from the respective animals were confirmed to be R20291 from PCR amplicons of
164 *CDR20291_1801* on *Tn6192* transposon in R20291 and *tcdA*; R20291Δ*feoB1* was further
165 confirmed from the absence of *feoB1* (**Fig S2**). Furthermore, there was no difference in *in vitro*
166 germination for R20291 and R20291Δ*feoB1* (**Fig S3**).
167
168 **Comparison of pathogenesis in mice, at fixed time points.** As the bioburdens in surviving
169 animals at day 10 strongly suggested R20291Δ*feoB1* inadequately colonized the large intestine,
170 we repeated our assessment at a shorter time point of 48 h. Several studies indicate that high fecal
171 bioburdens occur within 48 h of CDI in C57/BL6 mice and that this timepoint is suitable for
172 measuring inflammatory responses in CDI [24, 25]. Therefore, we compared the colonization and
173 pathogenesis of R20291Δ*feoB1* and R20291 over 48 h. After inducing dysbiosis with antibiotics
174 and DSS, 6 mice/group (3 males and 3 females) were infected with each strain. None of the animals
175 infected with either of the strains became moribund, but those infected with the WT had significant
176 weight loss when compared to the pre-infected weights (**Fig 3A**; p ≤0.01), whereas those infected

177 with the mutant gained weight ($p \leq 0.05$). Bioburdens of cecal contents revealed mice infected with
178 R20291Δ*feoB1* had almost 3-logs less bacteria, compared to mice infected with R20291 and this
179 was supported by bioburdens in feces taken at 24 and 48 h post-infection (**Fig 3B, C**); unpaired t-
180 test $p<0.0001$). Regarding toxins, ceca from WT infected mice had toxin titers of 10^2-10^3 (per
181 gram of cecal content), which was 1-2 logs (90-99%) greater than cecal toxin titers in mice infected
182 with R20291Δ*feoB1* (**Fig 3D**). Evaluation of inflammatory responses by qRT-PCR showed that
183 expression of pro-inflammatory tumor necrosis factor-alpha (TNF-α), granulocyte-macrophage
184 colony-stimulating factor (GM-CSF) and anti-inflammatory interleukin-10 (IL-10) were all
185 significantly lower in mice infected with R20291Δ*feoB1* (**Fig 3E**). While TNF-α and GM-CSF
186 promote neutrophil recruitment in CDI, the upregulation of IL-10 may occur to repress TNF-α and
187 GM-CSF [26]. Elevation of these three cytokines may be markers for CDI severity in the CDI
188 colitis model [23]. Overall, these findings indicate that *C. difficile* requires FeoB1 to colonize its
189 host and produce toxin-mediated disease symptoms.
190
191 ***C. difficile* adjust its metabolism to compensate for lack of FeoB1.** Transcriptomics was applied
192 to identify whether Δ*feoB1* altered the expression of metabolic pathways that affect toxin
193 production. RNA sequencing (RNA-seq) was done on R20291 and R20291Δ*feoB1* cultures taken
194 at mid-logarithmic (OD=0.3), late-logarithmic (OD=0.6) and stationary phase (OD=0.9). Genes
195 were significantly differentially expressed based on $p \leq 0.02$ and Log_2fold change (FC) ≥ 1.5 i.e.,
196 FC$\geq$2.8 following analysis in CLC Genomics Workbench version 12; **Table S1** list the expression
197 changes for all genes. **Table 1** highlights selected pathways/genes affected by Δ*feoB1*, including
198 genes that were identified at a less strict criteria of Log_2fold change (FC) ≥ 0.58 i.e., FC$\geq$1.5.
199 Across the three growth phases, there were 435 common differentially expressed genes, of which

200 151 were upregulated and 284 were downregulated (**Fig 4A**). Gene Ontology analysis revealed
201 Δ*feoB1* mostly affected redox and flavin-dependent processes (**Fig 4B, C**). Other differentially
202 regulated processes included carbohydrate metabolism, iron homeostasis, pathogenesis, flagellar
203 proteins, cell wall biosynthesis genes (**Fig 4B, C**). Although our studies were done in BHI media,
204 expression changes seen in our RNAseq are comparable to those reported for *C. difficile* CD630
205 *fur* mutant that was grown in low iron media [16]. As described below, we focused on analyzing
206 gene signatures that are linked to iron metabolism and *C. difficile* pathogenesis.
207
208 **Iron-responsive gene transcription.** Iron starvation in *C. difficile* increases the transcription of
209 flavodoxin (*fldx*), ferric uptake regulator (*fur*), riboflavin biosynthesis and alternate iron uptake
210 transporters [16]. In R20291Δ*feoB1* there was upregulation of the flavodoxin encoded by
211 *CDR20291_1925*; riboflavin biosynthesis genes *ribB* and *ribD*; and downregulation of
212 *CDR20291_2756*, encoding the iron storage protein bacterioferritin (**Fig 5**). Upregulation of
213 flavodoxin and riboflavin biosynthesis genes reflect a metabolic shift to adopt flavin cofactors, to
214 likely substitute for the iron-dependent ferredoxin. Furthermore, downregulation of
215 bacterioferritin suggests that cells sought to increase cellular availability of iron, by decreasing its
216 storage in bacterioferritin. Alternate iron acquisition transporters were also upregulated such as
217 ferrichrome-specific ABC transporter genes (*fhuC* and *fhuD*) (**Fig 5**), the low-affinity zinc
218 transporter ZupT and Feo2 genes (*feoA2* and *feoB2*) (**Table 1**). Increased expression of *zupT* also
219 occurs in *C. difficile* CD630 under iron limiting conditions [27] but it is unknown whether ZupT
220 transports iron as previously shown in *Escherichia coli* (20). Deletion of *zupT* in *C. difficile* was
221 reported to impair colonization in mice, although its effect on toxin production was not described
222 [28]. In iron-starved media, *C. difficile* CD630 WT and a *fur* mutant were reported to upregulate

223 polyamine biosynthesis genes, which led to the hypothesis that polyamines (e.g., spermidine) may
224 participate in acquiring and storing iron [16, 27]. However, in our transcriptome results, polyamine
225 biosynthesis genes were either downregulated or not significantly affected, but putative
226 transporters (e.g., CDR20291_3365) for polyamines were upregulated (**Table 1**).
227
228 **Relationship between FeoB1, pyruvate metabolism and toxin production.** In R20291Δ*feoB1*
229 (**Fig 6A**) PaLoc genes were significantly downregulated, including *tcdA* and *tcdB*, the sigma factor
230 *tcdR* and holin *tcdE* (**Table 1**). Thus, the low levels of TcdA and TcdB protein in supernatants
231 from R20291Δ*feoB1* directly correlate with repression of *tcdA* and *tcdB*. We recently reported that
232 Δ*feoB1* and disruption of iron-sulfur cluster biosynthesis caused pyruvate accumulation in non-
233 toxigenic ATCC 700057 [19]. In R20291Δ*feoB1* we also observed an accumulation of pyruvate
234 throughout the three growth phases, when compared to R20291 (**Fig 6B**). This was especially
235 pronounced in the stationary phase, where there was a 34.48% increase in pyruvate, compared to
236 7.84% and 11.94% in mid- and late-logarithmic cultures, respectively. Pyruvate feeds into multiple
237 metabolic pathways, where it can be converted to formate by pyruvate-formate lyase (Pfl); lactate
238 by lactate dehydrogenase (Ldh); acetyl-CoA by pyruvate-ferredoxin oxidoreductase (NifJ); or
239 enter the Krebs cycle to be converted to oxaloacetate by pyruvate carboxylase (Pyc) or malate by
240 malate dehydrogenase (Mdh) [29]. Our transcriptome data showed many of these genes were
241 differentially regulated (**Table 1**). In cultures at OD ~0.6 *pflD* and *pflE* were increased by 3.09-
242 and 3.39-fold respectively but were not significantly differentially expressed in stationary phase
243 cultures. In contrast, it was reported [16] that *pfl* genes were downregulated in a *C. difficile* CD630
244 *fur* mutant, which also accumulated pyruvate in chemically defined low iron media; upregulation
245 of *pfl* genes in our study may reflect differences in media used and types of mutants studied i.e.,

246 *fur* versus *feoB1*. Interestingly, *pyc* was more than two-fold downregulated in the transcriptome.
247 *C. difficile* encodes a partial Krebs cycle in which pyruvate is fed into the oxidative branch by Pyc
248 converting it to oxaloacetate, which is then converted to citrate, isocitrate and 2-oxoglutarate, with
249 the last two steps catalyzed by aconitase (*CDR20291_0763*) and isocitrate/3-isopropylmalate
250 dehydrogenase (*CDR20291_0764*). Oxaloacetate is thought to be metabolized to citrate by
251 homocitrate synthase (NifV), encoded by *CDR20291*_0762) [30]. These genes (*CDR20291_0762*
252 to *CDR20291_0764*) were all downregulated in the transcriptome (-1.89 to 12.93-fold across the
253 three growth phases [**Table 1**]). RT-qPCR of *pyc*, *CDR20291_0763* and *CDR20291_0764*
254 confirmed their downregulation (**Fig 6C**). Thus, it is likely that downregulation of *pyc* and the
255 oxidative branch of the Kreb cycle contributed to the build-up of pyruvate, which is known to
256 negatively affect transcription of *tcdA* and *tcdB* [9].
257 Other pathways associated with regulating toxin production were also upregulated.
258 Interestingly, cultures at OD ~0.6 showed statistically significant, but moderate, increases in
259 transcription of *prd* operon genes *prdA*, *prdB*, *prdC* and *prdF* (1.46-1.61-fold) that encode proteins
260 involved in the Stickland metabolism of proline (**Table 1**). Upregulation of Stickland enzymes is
261 also consistent with there being a shift to energy generating and redox balancing processes, which
262 may include enzymes that do not rely on ferredoxin [21]. Furthermore, activation of Stickland
263 reduction of proline is associated with repression of toxin production [13].
264

265 **CONCLUSION**
266
267 Within the oxygen-limited colon, the Feo system is crucial for intestinal pathogens since Fe^{2+} is
268 likely the dominant form of iron. This may explain why *C. difficile feoB1* is upregulated by >200-
269 fold in mice [31]. Our study clearly shows that *feoB1* is necessary for *C. difficile* to effectively

270 colonize and cause disease in mice. Although FeoB1 may be the main permease for ferrous iron
271 acquisition, its deletion did not affect *in vitro* growth of *C. difficile*. This is consistent with there
272 being various pathways for *C. difficile* to generate energy in a complex culture media. Such
273 pathways include fermentation of amino acids in the Stickland pathway in which the oxidation of
274 an amino acid (e.g., cysteine) is coupled to the reduction of another (e.g., proline) to produce ATP
275 [29]. Upregulation of the proline reductase operon in the transcriptome of mid-log cultures (**Table**
276 **1**) might also indicate that loss of *feoB1* in BHI media negatively impacted toxin production [11,
277 13]. Without Δ*feoB1*, *C. difficile* lacks *in vivo* fitness and could potentially be outcompeted by
278 other gut flora that also compete for available iron. Indeed, the Feo system is also essential for
279 other intestinal pathogens such as *E. coli*, *Helicobacter pylori* [32] and *Salmonella typhimurium*
280 [15], which encode a single FeoB homolog. For example, without the Feo system *S. typhimurium*
281 is unable to successfully colonize the large intestine of mice, but it can grow in blood and systemic
282 body sites [15]. Similarly, *H. pylori* requires the FeoB system to colonize mice gastric mucosa
283 though it encodes transporters for ferric iron and can acquire iron from host lactoferrin and
284 transferrin [32, 33]. Our findings suggest that even if other forms of iron were available at the site
285 of infection and/or *C. difficile* expressed other ferrous iron transporters (e.g., FeoB2 or ZupT),
286 FeoB1 appears to be indispensable for colonization and pathogenesis. In a *C. difficile* CD630 *fur*
287 mutant, iron starvation was shown to downregulate pili and flagella associated genes [16] that
288 contribute to *C. difficile* adherence and colonization. We also observed downregulation of the Type
289 IV pilin, surface layer protein A (*slpA*) and adhesin encoded by *cwp66* (**Table 1**). In *C. difficile*,
290 Type IV pilin contributes to cell-cell attachment in biofilms and adherence to epithelial cells; it
291 was reported that in strains CD630 and R20291, deletion of *pilB1* (*CD630_35120* and
292 *CDR20291_3349*) resulted in poorer colonization of mice colons and such mutants were

293 outcompeted by their WT parents [34]. Thus, the avirulence of R20291Δ*feoB1* in mice may be
294 multifactorial, possibly involving reductions of ferrous iron uptake, toxin production and
295 colonization of the gut epithelia.
296
297 Antivirulent strategies to treat CDI have primarily focused on inhibiting TcdA and TcdB, with
298 bezlotoxumab (monoclonal antibody to TcdB) being the only approved treatment [35]. However,
299 blocking the biosynthesis of TcdA and TcdB without inhibiting *in vitro* growth is an attractive
300 discovery-oriented approach for novel CDI therapeutics [36], which could complement existing
301 treatment approaches [35]. Given the rapidly increasing understanding of *C. difficile*
302 pathophysiology it may now be possible to target specific proteins and pathways that promote
303 toxin production [37]. In this regard, FeoB1 which is central to *C. difficile* metabolism and
304 pathogenesis could be a valuable drug target to discover novel CDI therapeutics.
305
306 **MATERIALS AND METHODS**
307 **Strains and culture conditions.** *C. difficile* R20291 and its isogenic *feoB1* deletion mutant
308 (R20291Δ*feoB1*) were routinely grown in pre-reduced BHI broth or agar at 37°C in a Whitley A35
309 anaerobic workstation (Don Whitley Scientific). *E. coli* SD46 was grown at 37°C in Luria–Bertani
310 (LB) broth or agar. D-cycloserine (250 μg/ml), cefoxitin (8 μg/ml), and thiamphenicol (15 μg/ml)
311 were used to selectively culture *C. difficile* containing plasmids, whereas chloramphenicol (15
312 μg/ml) and ampicillin (50 μg/ml) were used to grow *E. coli* SD46. Strains used are listed in **Table**
313 **S2**.
314

315 **Cell culture and conditions.** Vero epithelial cells were cultured in 10% fetal bovine serum and
316 Dulbecco's Modified Eagle Medium at 37°C with 5% carbon dioxide in a humidified incubator.
317 These culture conditions were used in cell rounding assays.
318
319 **Genetic manipulation of *C. difficile*.** R20291Δ*feoB1* was generated by allelic exchange, exactly
320 as we described (19). Essentially, *E. coli* SD46 carrying the *feoB1* allelic deletion cassette in
321 pMTL-SC7215 was conjugated into R20291, before subjecting the recombinant strain to serial
322 passage to select for double crossover mutants. The deletion was confirmed by PCR and Sanger
323 sequencing. R20291Δ*feoB1* was complemented with WT *feoB1* expressed from its promoter in
324 pMTL84151, as we described (19). The strain was maintained on pre-reduced BHI supplemented
325 with thiamphenicol (15 μg/ml). The primers used in the study are listed in **Table S3**.
326
327 **Quantification of *C. difficile* toxins.** Strains were grown anaerobically in pre-reduced BHI at
328 37°C for 24 h. Samples were centrifuged at 5000 rpm for 5 min and supernatants recovered for
329 ELISA and cell rounding assays, as follows. **(i) ELISA quantification.** About 100 μl of sample
330 was used to measure TcdA and TcdB using the tgcBIOMICS Gmbh ELISA kit that quantifies both
331 toxins, against standard curves from purified TcdA and TcdB, according to the manufacturer's
332 instructions. **(ii) Standard cell rounding assay.** Toxin titers were determined against Vero
333 epithelial cells (~10^5 cells/ml) that were adhered overnight. Supernatants from neat and various
334 diluted samples were added to the cells and incubated for 4 h. Cytopathic effects (cell rounding)
335 were visualized by microscopy, using six views per well. Toxin titers were defined as the lowest
336 dilution in which cell rounding was no longer visualized. (**iii) Determination of cell rounding by**
337 **morphometric analysis.** A similar approach was previously reported to quantify cell rounding in

338 a high throughput manner [22]. Briefly, 50 µl of 500-1000 Vero cells were seeded per well of a
339 384-well black plate and incubated for ~18 h. To generate a standard curve purified TcdB (List
340 Biological Laboratories, Inc) were diluted. From a source plate containing diluted TcdB and
341 undiluted culture supernatants 0.05 µl of samples were automatedly transferred to the 384-well
342 plate containing the Vero cells using Echo® Acoustic Liquid Handler. This represented an *in situ*
343 dilution of 1:1000 of the culture supernatants. Samples were incubated at 37°C for 6 h in 5%
344 carbon dioxide, followed by addition of 10 µl of 25% (v/v) paraformaldehyde. Cells were fixed
345 overnight at 4°C, washed with PBS and stained with the nucleic acid stain DAPI (25 µl). After
346 incubation in the dark for 15 min at room temperature, they were stained with Alexa Fluor 488
347 phalloidin strain (40 µl) at a concentration of 0.0006 µM in PBS with 5% milk powder solution.
348 After staining in the dark for 2 h, cells were washed twice, and PBS (50 µl) was added. Cell images
349 were captured using IN Cell Analyzer 6000 from GE Healthcare, with DAPI (excitation 358 nm
350 and emission 451 nm) and phalloidin (excitation 495 nm and emission 518 nm). Using Pipeline
351 Pilot version 9.2, automated morphometric analysis was done on: cell shape, coverage of the well
352 surface area by cells, perimeter, and circularity. From these parameters the percentage of rounded
353 cells were determined against the standard curve for TcdB.
354
355 **Quantification of toxins in mice ceca.** Cecal samples were collected and flash frozen. Samples
356 (normalized to g/ml) were homogenized in PBS containing cOmplete™ Protease Inhibitor
357 Cocktail from Roche, then centrifuged at 10, 000 rpm for 5 min. The supernatants (5 µl) were used
358 to quantify toxins by the above standard cell rounding assay.
359

360 **RNA Sequencing and analysis.** Triplicates of R20291 and R20291Δ*feoB1* were grown overnight
361 in pre-reduced BHI broth. The next day, cultures were diluted 1:100 in pre-reduced BHI broth and
362 grown in the anaerobic chamber. Approximately 20 ml samples of each strain were harvested at
363 three-time points OD~0.3, ~0.6, and ~0.9 and further aliquots of each time point also stored for
364 subsequent analyses. These time points were selected to assess changes in gene transcription at
365 different points in the bacterial growth cycle. Bacterial RNAprotect™ reagent (QIAGEN) was
366 added and RNA isolated using Qiagen's RNeasy mini kit. RNA quality assessment, library
367 preparation and Hi-Seq 2 x150 paired-end sequencing were performed by GENEWIZ (New Jersey,
368 USA).
369
370 **Analysis of RNA sequencing data.** CLC Genomics Workbench version 12.0 was used to analyze
371 RNA sequencing data. After trimming the adapters, the data was checked for its quality and
372 relatedness using Principal Component Analysis (PCA). Further, *C. difficile* R20291 coding
373 sequence (CDS, GenBank accession number: FN545816.1) was used for alignment and analysis.
374 Differential gene expression of R20291 Δ*feoB1* was analyzed against R20291 wild type. The raw
375 RNA-Seq data are deposited in NCBI database under accession number PRJNA753147.
376
377 **Transcriptional analysis by RT-qPCR.** RNA isolated from *C. difficile* samples was converted
378 to cDNA by M-MLV reverse transcriptase (Quantabio) using qScript cDNA SuperMix. qScript
379 One-Step SYBR Green qRT-PCR Kit, ROX (Quantabio) and gene-specific primers were used to
380 amplify genes in Applied Biosystems ViiA7 real-time PCR machine. Transcript levels were
381 calculated by the comparative Ct method (ΔΔCT method) and data normalized to 16S rRNA [38].
382 For analysis of cytokine levels in the cecal tissues, the same Qiagen's RNeasy mini kit was used

383 to isolate RNA and qRT-PCR was carried out as above. The data was normalized to the beta-actin
384 gene.
385
386 **Ethics statement**
387 Experiments were conducted under animal use protocol # 2018-0054-IBT, approved by the
388 Institutional Animal Care and Use Committee at Texas A&M University.
389
390 **Mouse model of colitis CDI.** The model of CDI was modified from that described by Zhou et al.
391 [23]. Male and female C57/BL6 mice (6 weeks) were from Envigo. For 5 days, mice were given
392 water containing kanamycin (0.4 µg/ml), gentamicin (0.035 µg/ml), colistin (850 U/ml),
393 metronidazole (0.215 µg/ml), vancomycin (0.045 µg/ml) and 1.5% w/v of dextran sodium sulfate.
394 This was followed by two days of regular drug-free water. On day-1, mice were injected (i.p.) with
395 clindamycin (10 mg/kg). Approximately 20 h later (day 0) they were infected with 10^5 spores of
396 either R20291 or R20291Δ*feoB1*. Three sets of experiments were carried out, as summarized in
397 the results. *C. difficile* spores were prepared according to a standard protocol [39]. After infection,
398 fecal samples were collected daily, and ceca recovered from euthanized moribund animals or at
399 the experimental endpoint. Animals were monitored three times per day and scored for: health
400 appearance, including hunched posture, ruffled fur, and diarrhea (wet tail); weight loss; and
401 decreases in body temperature (**Table S4**). Moribund animals were compassionately sacrificed.
402
403 **Analysis of cecal and fecal bioburdens.** Samples were weighed, homogenized in PBS and
404 normalized to g/ml. To enumerate spore burdens, samples were heated at 70ºC for 30 minutes,
405 diluted and then plated onto *C. difficile* selection agar (containing cycloserine, cefoxitin, and

406 fructose) supplemented with 0.1% w/v sodium taurocholate. After anaerobic incubation for up to
407 48 h viable counts were determined.
408
409 **Quantification of intracellular iron by ICP-OES.** Overnight grown cells were subcultured
410 (1:100) in fresh BHI broth and harvested after 6 h for ICP-OES analysis to determine the cellular
411 iron levels as we previously described [19].
412
413 **Quantification of intracellular pyruvate.** This assay was performed as we previously described
414 [19]; essentially harvesting samples at OD~0.3, 0.6 and 0.9 to measuring intracellular pyruvate in
415 cell lysates using the Pyruvate Colorimetric/Fluorometric Assay kit from Biovision.
416
417
418 **ACKNOWLEDGEMENTS**
419 This work was in part funded by grants R56AI126881 and R01AI139261 to J.G.H. from the
420 National Institute of Allergy and Infectious Diseases at the National Institutes of Health. The
421 funders had no role in study design, in data collection and interpretation of the findings, or in the
422 writing and submission of the manuscript.

423 **REFERENCES**

424 1. Guh AY, Mu Y, Winston LG, Johnston H, Olson D, Farley MM, et al. Trends in U.S.
425 Burden of Clostridioides difficile Infection and Outcomes. N Engl J Med. 2020;382(14):1320-
426 30. Epub 2020/04/04. doi: 10.1056/NEJMoa1910215. PubMed PMID: 32242357; PubMed
427 Central PMCID: PMCPMC7861882.

428 2. Rupnik M, Wilcox MH, Gerding DN. Clostridium difficile infection: new developments
429 in epidemiology and pathogenesis. Nat Rev Microbiol. 2009;7(7):526-36. Epub 2009/06/17. doi:
430 nrmicro2164 [pii]
431 10.1038/nrmicro2164. PubMed PMID: 19528959.

432 3. Lessa FC, Mu Y, Bamberg WM, Beldavs ZG, Dumyati GK, Dunn JR, et al. Burden of
433 Clostridium difficile infection in the United States. N Engl J Med. 2015;372(9):825-34. doi:
434 10.1056/NEJMoa1408913. PubMed PMID: 25714160.

435 4. Louie TJ, Miller MA, Mullane KM, Weiss K, Lentnek A, Golan Y, et al. Fidaxomicin
436 versus vancomycin for Clostridium difficile infection. N Engl J Med. 2011;364(5):422-31. Epub
437 2011/02/04. doi: 10.1056/NEJMoa0910812. PubMed PMID: 21288078.

438 5. Louie TJ, Miller MA, Mullane KM, Weiss K, Lentnek A, Golan Y, et al. Fidaxomicin
439 versus vancomycin for Clostridium difficile infection. N Engl J Med. 2011;364(5):422-31. Epub
440 2011/02/04. doi: 10.1056/NEJMoa0910812. PubMed PMID: 21288078.

441 6. Chandrasekaran R, Lacy DB. The role of toxins in Clostridium difficile infection. FEMS
442 Microbiol Rev. 2017;41(6):723-50. Epub 2017/10/20. doi: 10.1093/femsre/fux048. PubMed
443 PMID: 29048477; PubMed Central PMCID: PMCPMC5812492.

444 7. Antunes A, Camiade E, Monot M, Courtois E, Barbut F, Sernova NV, et al. Global
445 transcriptional control by glucose and carbon regulator CcpA in Clostridium difficile. Nucleic

446 Acids Res. 2012;40(21):10701-18. doi: 10.1093/nar/gks864. PubMed PMID: 22989714; PubMed
447 Central PMCID: PMC3510511.
448 8. Karlsson S, Burman LG, Akerlund T. Suppression of toxin production in Clostridium
449 difficile VPI 10463 by amino acids. Microbiology. 1999;145 (Pt 7):1683-93. Epub 1999/08/10.
450 doi: 10.1099/13500872-145-7-1683. PubMed PMID: 10439407.
451 9. Dubois T, Dancer-Thibonnier M, Monot M, Hamiot A, Bouillaut L, Soutourina O, et al.
452 Control of Clostridium difficile Physiopathology in Response to Cysteine Availability. Infect
453 Immun. 2016;84(8):2389-405. Epub 2016/06/15. doi: 10.1128/IAI.00121-16. PubMed PMID:
454 27297391; PubMed Central PMCID: PMCPMC4962627.
455 10. Dineen SS, Villapakkam AC, Nordman JT, Sonenshein AL. Repression of Clostridium
456 difficile toxin gene expression by CodY. Mol Microbiol. 2007;66(1):206-19. Epub 2007/08/30.
457 doi: 10.1111/j.1365-2958.2007.05906.x. PubMed PMID: 17725558.
458 11. Bouillaut L, Dubois T, Francis MB, Daou N, Monot M, Sorg JA, et al. Role of the global
459 regulator Rex in control of NAD(+) -regeneration in Clostridioides (Clostridium) difficile. Mol
460 Microbiol. 2019;111(6):1671-88. Epub 2019/03/19. doi: 10.1111/mmi.14245. PubMed PMID:
461 30882947; PubMed Central PMCID: PMCPMC6561804.
462 12. Martin-Verstraete I, Peltier J, Dupuy B. The Regulatory Networks That Control
463 Clostridium difficile Toxin Synthesis. Toxins (Basel). 2016;8(5). Epub 2016/05/18. doi:
464 10.3390/toxins8050153. PubMed PMID: 27187475; PubMed Central PMCID:
465 PMCPMC4885068.
466 13. Bouillaut L, Dubois T, Sonenshein AL, Dupuy B. Integration of metabolism and
467 virulence in Clostridium difficile. Res Microbiol. 2015;166(4):375-83. Epub 2014/12/03. doi:

468 10.1016/j.resmic.2014.10.002. PubMed PMID: 25445566; PubMed Central PMCID:
469 PMCPMC4398617.
470 14. Lau CK, Krewulak KD, Vogel HJ. Bacterial ferrous iron transport: the Feo system.
471 FEMS Microbiol Rev. 2016;40(2):273-98. Epub 2015/12/20. doi: 10.1093/femsre/fuv049.
472 PubMed PMID: 26684538.
473 15. Tsolis RM, Baumler AJ, Heffron F, Stojiljkovic I. Contribution of TonB- and Feo-
474 mediated iron uptake to growth of Salmonella typhimurium in the mouse. Infect Immun.
475 1996;64(11):4549-56. Epub 1996/11/01. PubMed PMID: 8890205; PubMed Central PMCID:
476 PMCPMC174411.
477 16. Berges M, Michel AM, Lassek C, Nuss AM, Beckstette M, Dersch P, et al. Iron
478 Regulation in Clostridioides difficile. Front Microbiol. 2018;9:3183. Epub 2019/01/09. doi:
479 10.3389/fmicb.2018.03183. PubMed PMID: 30619231; PubMed Central PMCID:
480 PMCPMC6311696.
481 17. Ho TD, Ellermeier CD. Ferric Uptake Regulator Fur Control of Putative Iron Acquisition
482 Systems in Clostridium difficile. J Bacteriol. 2015;197(18):2930-40. doi: 10.1128/JB.00098-15.
483 PubMed PMID: 26148711; PubMed Central PMCID: PMCPMC4542176.
484 18. Awad MM, Cheung JK, Tan JE, McEwan AG, Lyras D, Rood JI. Functional analysis of
485 an feoB mutant in Clostridium perfringens strain 13. Anaerobe. 2016;41:10-7. Epub 2016/05/15.
486 doi: 10.1016/j.anaerobe.2016.05.005. PubMed PMID: 27178230.
487 19. Deshpande A, Wu X, Huo W, Palmer KL, Hurdle JG. Chromosomal Resistance to
488 Metronidazole in Clostridioides difficile can be Mediated by Epistasis Between Iron
489 Homeostasis and Oxidoreductases. Antimicrob Agents Chemother. 2020. Epub 2020/05/28. doi:
490 10.1128/AAC.00415-20. PubMed PMID: 32457109.

491 20. Stabler RA, He M, Dawson L, Martin M, Valiente E, Corton C, et al. Comparative
492 genome and phenotypic analysis of Clostridium difficile 027 strains provides insight into the
493 evolution of a hypervirulent bacterium. Genome Biol. 2009;10(9):R102. Epub 2009/09/29. doi:
494 10.1186/gb-2009-10-9-r102. PubMed PMID: 19781061; PubMed Central PMCID:
495 PMCPMC2768977.
496 21. Marreddy RKR, Olaitan AO, May JN, Dong M, Hurdle JG. Ebselen Not Only Inhibits
497 Clostridioides difficile Toxins but Displays Redox-Associated Cellular Killing. Microbiol
498 Spectr. 2021:e0044821. Epub 2021/09/02. doi: 10.1128/Spectrum.00448-21. PubMed PMID:
499 34468187.
500 22. Xie J, Horton M, Zorman J, Antonello JM, Zhang Y, Arnold BA, et al. Development and
501 optimization of a high-throughput assay to measure neutralizing antibodies against Clostridium
502 difficile binary toxin. Clin Vaccine Immunol. 2014;21(5):689-97. Epub 2014/03/14. doi:
503 10.1128/CVI.00038-14. PubMed PMID: 24623624; PubMed Central PMCID:
504 PMCPMC4018877.
505 23. Zhou F, Hamza T, Fleur AS, Zhang Y, Yu H, Chen K, et al. Mice with Inflammatory
506 Bowel Disease are Susceptible to Clostridium difficile Infection With Severe Disease Outcomes.
507 Inflamm Bowel Dis. 2018;24(3):573-82. Epub 2018/02/21. doi: 10.1093/ibd/izx059. PubMed
508 PMID: 29462386; PubMed Central PMCID: PMCPMC5936643.
509 24. Collins J, Robinson C, Danhof H, Knetsch CW, van Leeuwen HC, Lawley TD, et al.
510 Dietary trehalose enhances virulence of epidemic Clostridium difficile. Nature.
511 2018;553(7688):291-4. Epub 2018/01/09. doi: 10.1038/nature25178. PubMed PMID: 29310122.

512 25. Howerton A, Patra M, Abel-Santos E. A new strategy for the prevention of Clostridium
513 difficile infection. J Infect Dis. 2013;207(10):1498-504. Epub 2013/02/20. doi:
514 10.1093/infdis/jit068. PubMed PMID: 23420906.
515 26. McDermott AJ, Frank CR, Falkowski NR, McDonald RA, Young VB, Huffnagle GB.
516 Role of GM-CSF in the inflammatory cytokine network that regulates neutrophil influx into the
517 colonic mucosa during Clostridium difficile infection in mice. Gut Microbes. 2014;5(4):476-84.
518 Epub 2014/07/22. doi: 10.4161/gmic.29964. PubMed PMID: 25045999; PubMed Central
519 PMCID: PMCPMC5915364.
520 27. Hastie JL, Hanna PC, Carlson PE. Transcriptional response of Clostridium difficile to
521 low iron conditions. Pathog Dis. 2018;76(2). Epub 2018/02/02. doi: 10.1093/femspd/fty009.
522 PubMed PMID: 29390127; PubMed Central PMCID: PMCPMC6251574.
523 28. Zackular JP, Knippel RJ, Lopez CA, Beavers WN, Maxwell CN, Chazin WJ, et al. ZupT
524 Facilitates Clostridioides difficile Resistance to Host-Mediated Nutritional Immunity. mSphere.
525 2020;5(2). Epub 2020/03/13. doi: 10.1128/mSphere.00061-20. PubMed PMID: 32161145;
526 PubMed Central PMCID: PMCPMC7067591.
527 29. Neumann-Schaal M, Jahn D, Schmidt-Hohagen K. Metabolism the Difficile Way: The
528 Key to the Success of the Pathogen Clostridioides difficile. Front Microbiol. 2019;10:219. Epub
529 2019/03/05. doi: 10.3389/fmicb.2019.00219. PubMed PMID: 30828322; PubMed Central
530 PMCID: PMCPMC6384274.
531 30. Li F, Hagemeier CH, Seedorf H, Gottschalk G, Thauer RK. Re-citrate synthase from
532 Clostridium kluyveri is phylogenetically related to homocitrate synthase and isopropylmalate
533 synthase rather than to Si-citrate synthase. J Bacteriol. 2007;189(11):4299-304. Epub 20070330.

534 doi: 10.1128/JB.00198-07. PubMed PMID: 17400742; PubMed Central PMCID:
535 PMCPMC1913417.
536 31. Fletcher JR, Erwin S, Lanzas C, Theriot CM. Shifts in the Gut Metabolome and
537 Clostridium difficile Transcriptome throughout Colonization and Infection in a Mouse Model.
538 mSphere. 2018;3(2). Epub 2018/03/31. doi: 10.1128/mSphere.00089-18. PubMed PMID:
539 29600278; PubMed Central PMCID: PMCPMC5874438.
540 32. Velayudhan J, Hughes NJ, McColm AA, Bagshaw J, Clayton CL, Andrews SC, et al.
541 Iron acquisition and virulence in Helicobacter pylori: a major role for FeoB, a high-affinity
542 ferrous iron transporter. Mol Microbiol. 2000;37(2):274-86. Epub 2000/08/10. doi:
543 10.1046/j.1365-2958.2000.01987.x. PubMed PMID: 10931324.
544 33. Senkovich O, Ceaser S, McGee DJ, Testerman TL. Unique host iron utilization
545 mechanisms of Helicobacter pylori revealed with iron-deficient chemically defined media. Infect
546 Immun. 2010;78(5):1841-9. Epub 2010/02/24. doi: 10.1128/IAI.01258-09. PubMed PMID:
547 20176792; PubMed Central PMCID: PMCPMC2863533.
548 34. McKee RW, Aleksanyan N, Garrett EM, Tamayo R. Type IV Pili Promote Clostridium
549 difficile Adherence and Persistence in a Mouse Model of Infection. Infect Immun. 2018;86(5).
550 Epub 20180423. doi: 10.1128/IAI.00943-17. PubMed PMID: 29483294; PubMed Central
551 PMCID: PMCPMC5913833.
552 35. Johnson S, Lavergne V, Skinner AM, Gonzales-Luna AJ, Garey KW, Kelly CP, et al.
553 Clinical Practice Guideline by the Infectious Diseases Society of America (IDSA) and Society
554 for Healthcare Epidemiology of America (SHEA): 2021 Focused Update Guidelines on
555 Management of Clostridioides difficile Infection in Adults. Clin Infect Dis. 2021;73(5):755-7.
556 doi: 10.1093/cid/ciab718. PubMed PMID: 34492699.

557 36. Thanissery R, Zeng D, Doyle RG, Theriot CM. A Small Molecule-Screening Pipeline to
558 Evaluate the Therapeutic Potential of 2-Aminoimidazole Molecules Against Clostridium
559 difficile. Front Microbiol. 2018;9:1206. Epub 2018/06/22. doi: 10.3389/fmicb.2018.01206.
560 PubMed PMID: 29928268; PubMed Central PMCID: PMCPMC5997789.
561 37. Hofmann JD, Otto A, Berges M, Biedendieck R, Michel AM, Becher D, et al. Metabolic
562 Reprogramming of Clostridioides difficile During the Stationary Phase With the Induction of
563 Toxin Production. Front Microbiol. 2018;9:1970. Epub 2018/09/07. doi:
564 10.3389/fmicb.2018.01970. PubMed PMID: 30186274; PubMed Central PMCID:
565 PMCPMC6110889.
566 38. Livak KJ, Schmittgen TD. Analysis of relative gene expression data using real-time
567 quantitative PCR and the 2(-Delta Delta C(T)) Method. Methods. 2001;25(4):402-8. doi:
568 10.1006/meth.2001.1262. PubMed PMID: 11846609.
569 39. Edwards AN, McBride SM. Isolating and Purifying Clostridium difficile Spores.
570 Methods Mol Biol. 2016;1476:117-28. Epub 2016/08/11. doi: 10.1007/978-1-4939-6361-4_9.
571 PubMed PMID: 27507337; PubMed Central PMCID: PMCPMC5017156.
572
573
574
575
576
577
578
579

580 **TABLES AND FIGURES**

581 **Table 1.** Selected genes[a] in *C. difficile* R20291 that were differentially expressed in

582 R20291Δ*feoB1* compared to WT R20291.

Functional group/proteins	**Gene**	**Δ*feoB1* vs WT (Log2(FC) ≥0.58)**		
		Mid log	**Late log**	**Stationary**
Flavodoxin, iron metabolism and metal transport				
Flavodoxin	*fldx (CDR20291_1925)*	4.33	3.87	2.91
Riboflavin synthase beta-chain	*ribH (CDR20291_1595)*			1.34
Riboflavin synthase alpha chain	*ribB (CDR20291_1597)*	1.27	1.41	1.52
Riboflavin biosynthesis bifunctional diaminohydroxyphosphoribosylaminopyrimidine deaminase and 5-amino-6-(5-phosphoribosylamino)uracil reductase]	*ribD (CDR20291_1598)*	1.19	1.24	1.61
Bacterioferritin	*bfr (CDR20291_2756)*	-2.9	-2.57	-2.53
Ferrichrome- specific ABC transporter permease, ATP-binding protein	*fhuC (CDR20291_2771)*	0.92	0.73	
Ferrichrome- specific ABC transporter permease, substrate binding protein	*fhuD (CDR20291_2774)*	1.16		-1.52
Zinc Transporter	*zupT (CDR20291_0946)*	1.42	0.83	1.63
ABC-type Fe3+ transport system, permease component	*CDR20291_2980*	-7.61	-7.37	-7.91
ABC-type spermidine/putrescine transport systems, ATPase component	*CDR20291_2981*	-7.19	-7.55	-8.09
Iron (III) transport system substrate-binding protein	*CDR20291_2983*	-7.1	-7.51	-8.46

ABC-type Fe3+ transport system, solute-binding protein	*CDR20291_3362*	2.83	2.62	2.38
ABC-type Fe3+ transport system, permease component	*CDR20291_3364*	4.39	4.29	4.12
ABC-type Fe3+ transport system, ATPase component (polyamine transport)	*CDR20291_3365*	4.11	4.59	3.7
Ferrous iron transporter subunit A2	*feoA2 (CDR20291_1367)*	3.06	3	1.81
Ferrous iron transporter subunit B2	*feoB2 (CDR20291_1366)*	2.05	1.91	1.90
Cobalt ABC transporter, ATP-binding protein	*cbiO (CDR20291_0332)*	0.91	1.51	
Polyamine biosynthesis				
S-adenosylmethionine decarboxylase	*speD (CDR20291_0819)*	-1.27	-0.96	-1.2
Spermidine synthase	*speE* (*CDR20291_0820*)	-0.69		
Energy metabolism				
Pyruvate carboxylase	*pyc (CDR20291_0010)*	-1.31	-1.4	-1.14
Pyruvate formate lyase	*pflD (CDR20291_3143)*		1.63	
Pyruvate-formate lyase-activating enzyme	*pflE (CDR20291_3144)*	0.87	1.76	
Homocitrate synthase NifV-type	*CDR20291_0762*	-3.11	-1.55	-3.69
Aconitase/3-isopropylmalate dehydratase	*CDR20291_0763*	-2.35	-2.47	-2.58
Isocitrate/3-isopropylmalate dehydrogenase	*CDR20291_0764*	-2.58	-1.89	-2.85
Succinyl-CoA:coenzyme A transferase	*cat1 (CDR20291_2232)*	6.19	6.55	5.38
Succinate-semialdehyde dehydrogenase [NAD(P)+]	*sucD (CDR20291_2231)*	6.39	6.74	5.48
Electron transfer flavoprotein alpha-subunit	*etfA2 (CDR20291_0912)*	1.64	2.42	1.91
Electron transfer flavoprotein beta-subunit	*etfB2 (CDR20291_0911)*		1.78	
Acetyl-CoA acetyltransferase	*thlA1 (CDR20291_0915)*		2.08	

3-hydroxybutyryl-CoA dehydratase	*crt2 (CDR20291_0913)*	1.14	2.11	1.53
Butyryl-CoA dehydrogenase complex	*bcd2 (CDR20291_0910)*		1.76	
Maltose phosphorylase	*mapA (CDR20291_2094)*	1.4	1.49	1.31
Maltose/glucose PTS system EIICB component	*CDR20291_2402*	1.8	1.86	1.95
Carbon catabolite repressor protein A	*ccpA (CDR20291_0923)*	0.77		
Proline reductase				
Proline reductase subunit proprotein	*prdA (CDR20291_3103)*		0.57	
Proline reductase	*prdB (CDR20291_3101)*		0.65	
Putative electron transfer protein	*prdC (CDR20291_3105)*		0.54	
Proline racemase	*prdF (CDR20291_3097)*		0.69	
Pathogenicity locus (PaLoc)				
Toxin A	*tcdA (CDR20291_0584)*	-6.64	-6.53	-9.47
Toxin B	*tcdB (CDR20291_0582)*	-6.14	-6.21	-8.94
Positive toxin regulator	*tcdR (CDR20291_0581)*	-4.51	-4.9	-6.15
Holin-like protein	*tcdE (CDR20291_0583)*	-5.63	-6.36	-7.83
Surface proteins and Pili				
Cell surface protein	*cwp66 (CDR20291_2678)*		-0.59	
Surface layer protein A	*slpA (CDR20291_2682)*	-2.26	-2.1	-2.35
Type IV prepilin leader peptidase	*CDR20291_3340*	-0.78	-1.2	0.19
Type IV prepilin leader peptidase	*CDR20291_3341*	-0.96	-0.75	-1.01
Type IV pilus retraction protein	*CDR20291_3342*	-0.83	-0.65	
Type IV pilin	*CDR20291_3345*	-0.67	-0.78	
Type IV pilus assembly protein	*CDR20291_3346*	-0.64		
Type IV pilus assembly protein	*CDR20291_3348*	-0.73	-0.89	

Type IV pilus assembly protein	*CDR20291_3349*	-0.73

583

584 [a]The above genes were selected from **Table S1** for the following reasons: (i) Representation of
585 pathways affected by iron limitation in cells, including iron and metal acquisition transporters
586 and indicative of shift to flavodoxin metabolism (supported by riboflavin biosynthesis) and
587 energy metabolism pathways; (ii) indication that polyamine biosynthesis was not enhanced as a
588 means to acquire iron in BHI; and (iii) pathogenicity was affected in terms of expression of
589 PaLoc genes and surface proteins that help *C. difficile* to colonize the large bowel. Log2Fold
590 changes are based on $p \leq 0.02$.

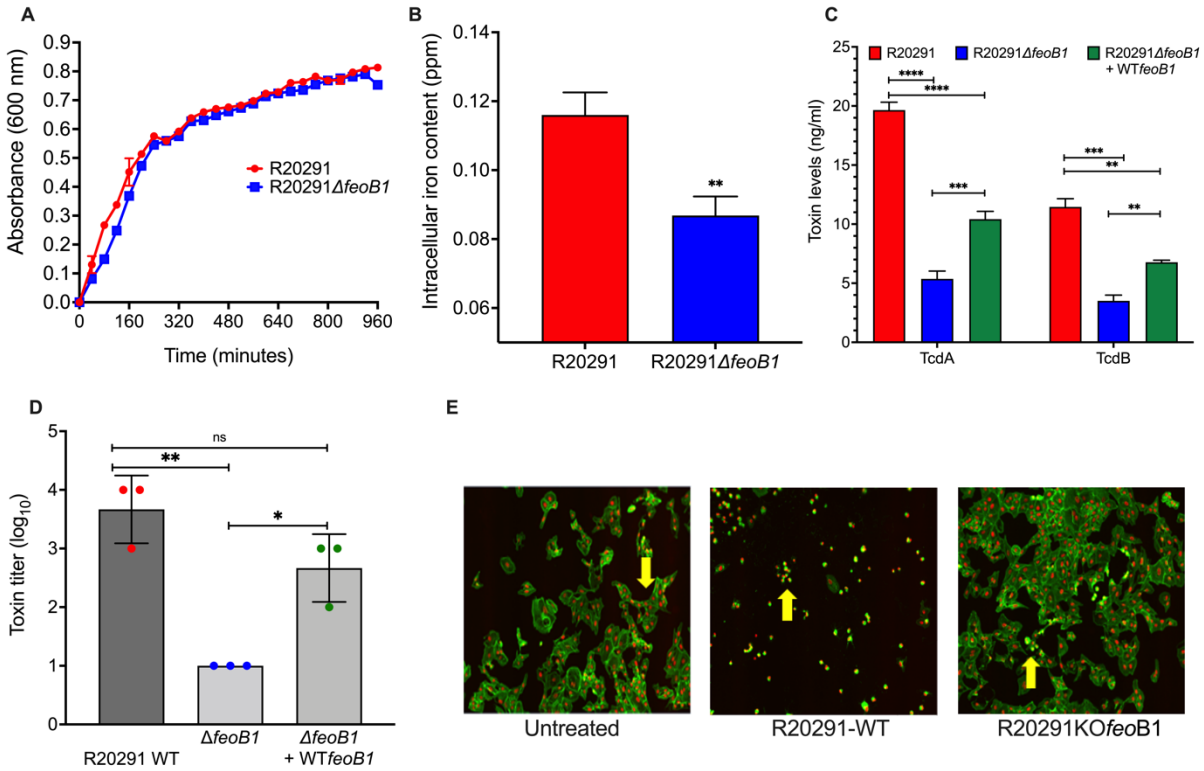

591

592

593 **Figure 1. Deletion of *feoB1* attenuates toxin production in *C. difficile* R20291. A.** Loss of *feoB1*
594 did not affect the growth of R20291. **B.** Without FeoB1, there was a ~ 25% reduction in
595 intracellular iron content in R20291Δ*feoB1*. The amounts of toxins TcdA and TcdB were
596 diminished in R20291Δ*feoB1* as determined by manual cell rounding analysis in **C**, showing toxin
597 titers against Vero epithelial cells and in **D**, quantification of toxins by ELISA. Based on the more
598 sensitive cell rounding assay, there was ~ 1000-fold less toxins produced by the mutant. Vero cells
599 are more predictive for cell rounding caused by TcdB. **E.** These results were confirmed by
600 automated morphometric analysis. Images show that more cell rounding was caused by the neat
601 supernatant of WT R20291 than that of the mutant (1:1000 *in situ* dilution). In the untreated
602 control, the yellow arrow shows the morphology of Vero cells, of actin filaments stained with
603 phalloidin (green) and nuclei stained with DAPI (red); in cells treated with WT supernatants, the

604 yellow arrow shows the morphology of rounded cells. In cells treated with supernatants from the
605 mutant, most cells appeared healthy. Statistical significance was determined by unpaired t-tests
606 with Welch's correction in Graphpad Prism 9.0; asterisks correspond to p values of * $p \leq 0.05$, **
607 $p \leq 0.01$, *** $p \leq 0.001$, **** $p < 0.0001$; ns=not significant $p > 0.05$.
608
609
610
611
612
613
614
615
616
617
618
619
620
621
622
623
624
625

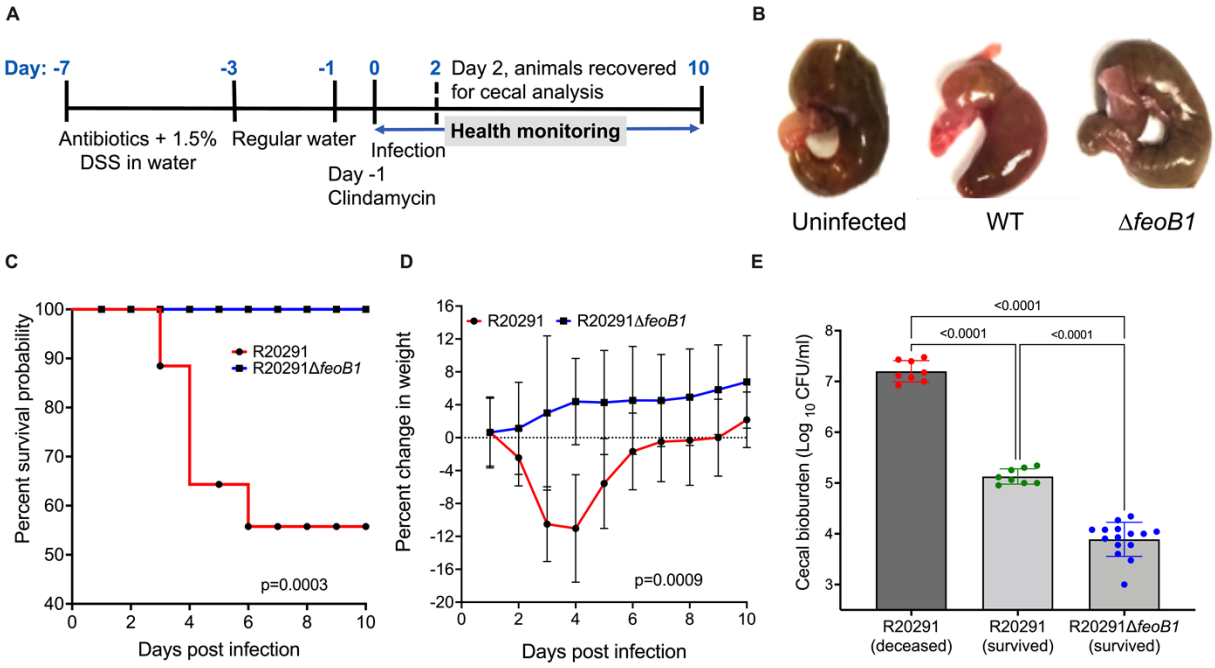

Figure 2. Deletion of FeoB1 attenuates colonization and virulence in mice. A. Schematic of the experimental timeline and procedure summary of the colitis CDI model used to evaluate the pathogenesis of R20291 and R20291Δ*feoB1*. **B.** Ceca recovered from the mice infected with the wild type were red and inflamed in contrast to that from the *feoB1* mutant, which resembled the uninfected control mice ceca. **C.** Kaplan-Meier survival analysis revealed significant difference (p=0.0003) between mortality risks of mice infected with R20291 compared to R20291Δ*feoB1*. **D.** Animals infected with R20291 exhibited significant weight loss (p=0.0009) compared to those infected with R20291Δ*feoB1*. **E**. Endpoint cecal bioburdens revealed that deceased mice infected with R20291 had higher bacterial loads than mice that survived infection with R20291, while mice infected with the mutant R20291Δ*feoB1* had even lower bioburdens. Data above are based on group numbers of n=16 mice infected with R20291 and n=15 mice infected with R20291Δ*feoB1* (a mouse from the R20291Δ*feoB1* group was removed from the study, as it was inadvertently infected with R20291, as confirmed by PCR on cecal isolates). Statistical significance for Kaplan-

640 Meier survival were determined by log-rank test in Graphpad Prism 9.0. Results in E were
641 analyzed by one-way ANOVA with alpha 0.05 in Graphpad Prism 9.0. Other statistical analyses
642 were determined by unpaired t-tests with Welch's correction in Graphpad Prism 9.0.
643

644

645

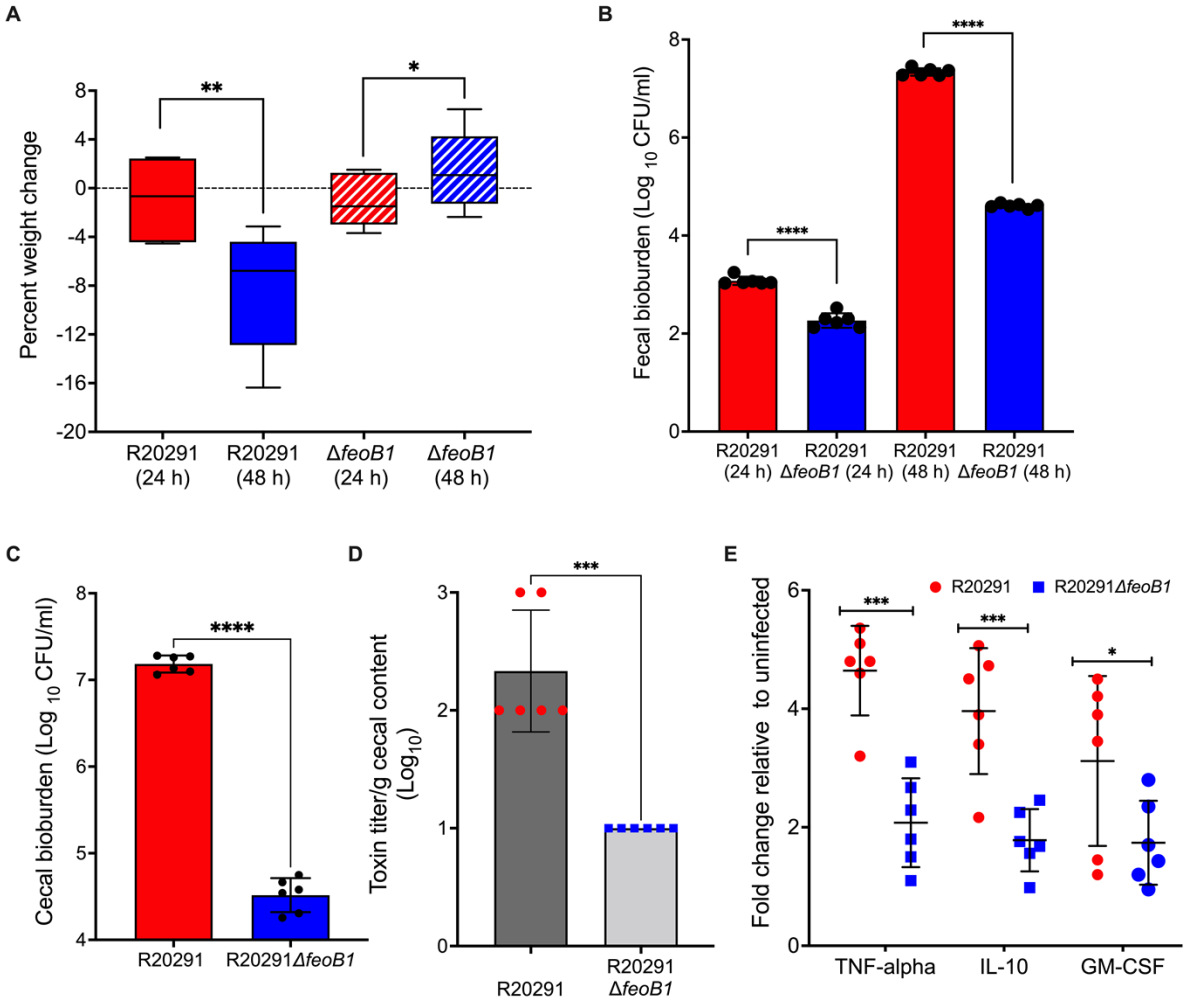

646

647 **Figure 3. Comparative analysis of virulence in mice at 48 h post-infection. A.** Significant
648 weight loss was seen 48 hours after infection with R20291 whereas mice infected with
649 R20291Δ*feoB1* gained weight, which was also significant. **B, C.** Reduced colonization by
650 R20291Δ*feoB1* was also evident from bioburdens analyzed from the ceca taken at 48 hours and
651 fecal samples recovered at 24 and 48 h. **D, E.** Lower toxin titers and expression of cytokine in
652 cecal tissues were also evident. Statistical significance was determined by unpaired t-tests with

653 Welch's correction in Graphpad Prism 9.0; asterisks correspond to p values of * p ≤0.05, ** p

654 ≤0.01, *** p ≤0.001, **** p<0.0001; ns=not significant p>0.05.

655

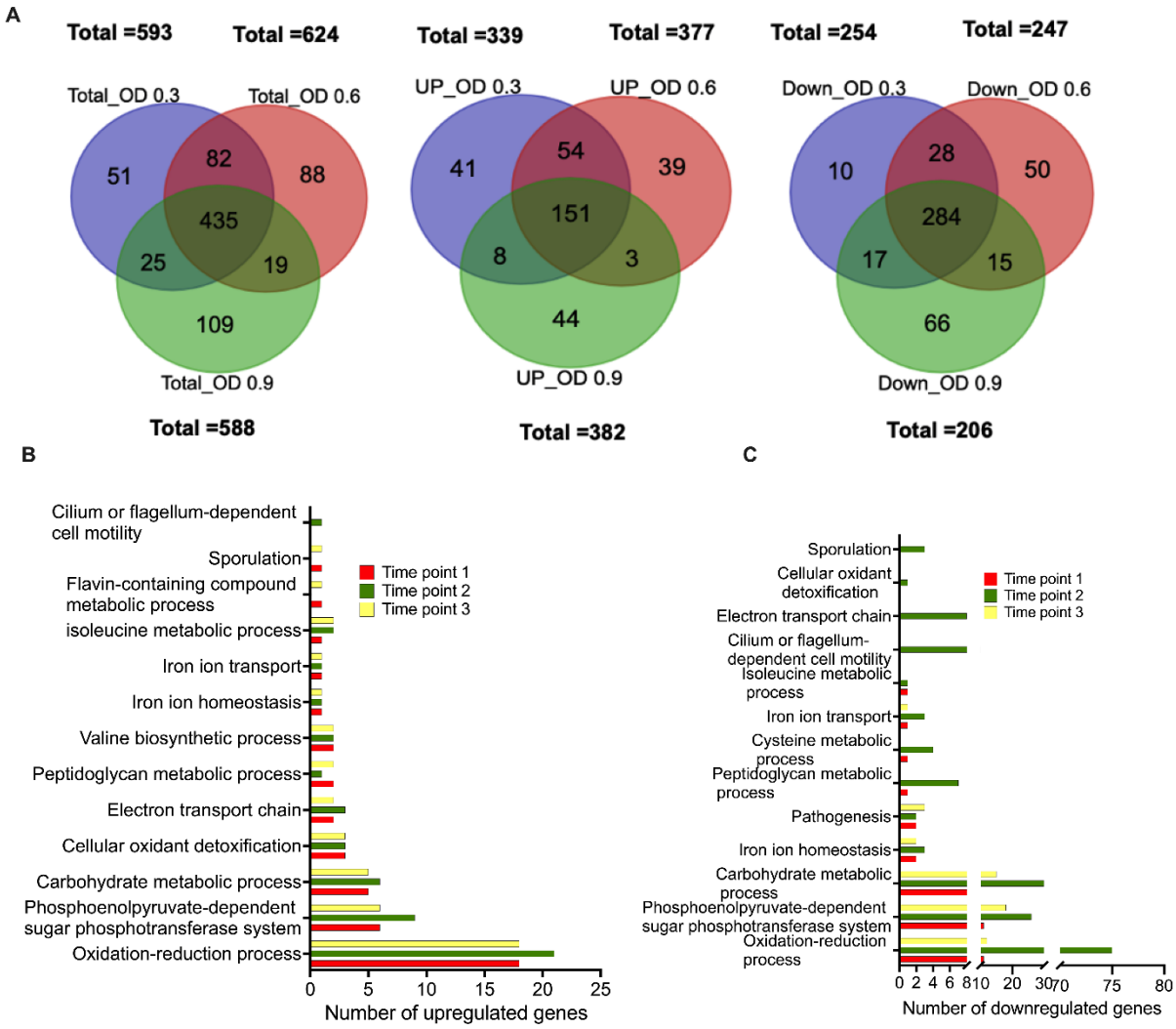

656

657

658 **Figure 4. Transcriptome changes associated with lack of *feoB1* in R20291. A.** Venn diagrams

659 show total differentially expressed genes (DEGs) and those that were upregulated or

660 downregulated at different growth phases (mid logarithmic OD600nm=0.3; late-logarithmic

661 OD600nm=0.6; and stationary phase OD600nm=0.9). **B, C**. Gene Ontology analysis of DEGs

662 identify different metabolic processes that are likely altered by loss of *feoB1*, including iron
663 homeostasis, pathogenesis, and redox reactions.
664

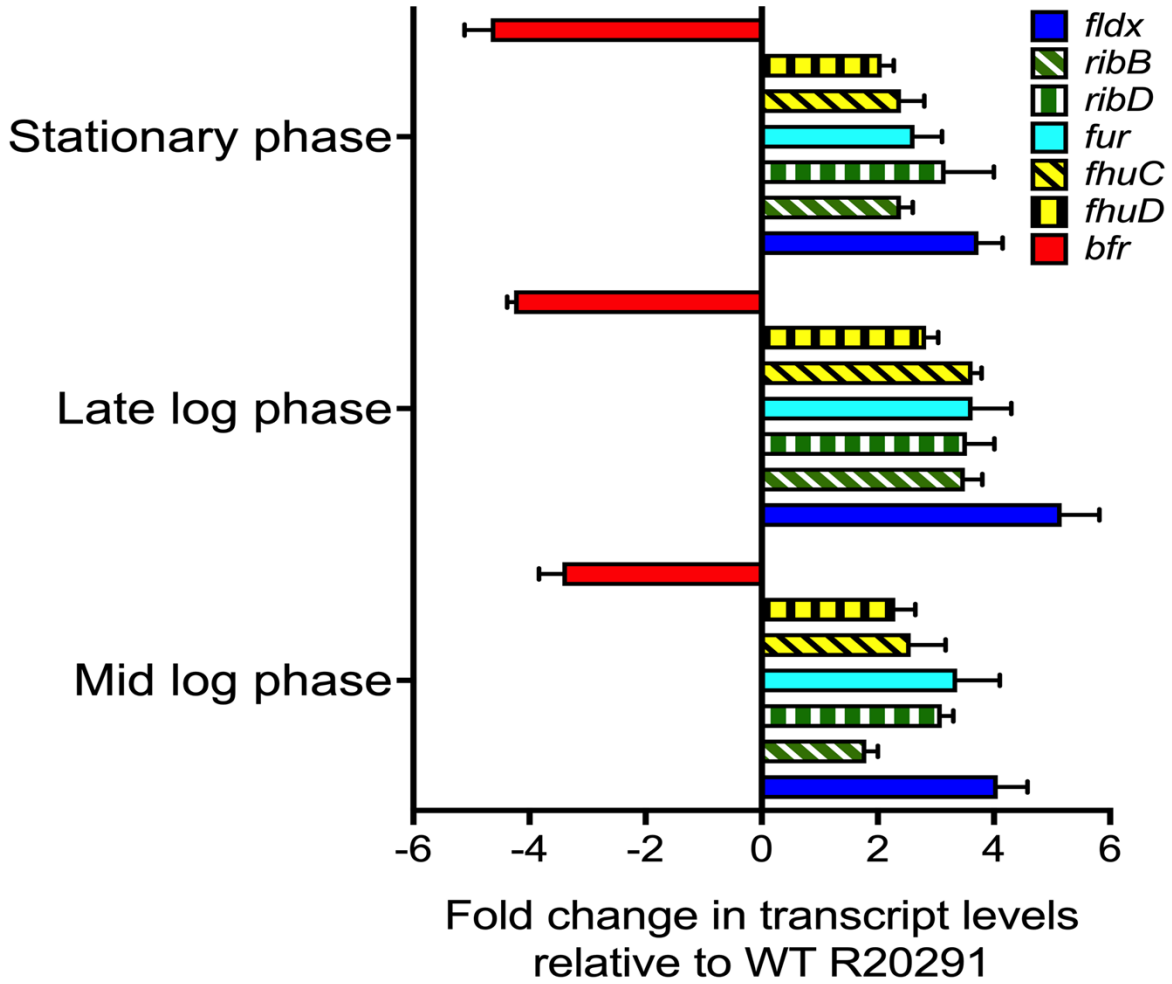

665
666 **Figure 5. Effect of loss of FeoB1 on iron-responsive gene transcription, as determined by RT-**
667 **qPCR.** Reduced iron uptake triggered genes involved in iron metabolism; upregulated were
668 flavodoxin (*fldx*), ferrichrome-specific ABC transporter permease (*fhuC* and *fhuD*), ferric uptake
669 regulator (*fur*) and riboflavin biosynthesis genes (*ribB* and *ribD*), while bacterioferritin (*bfr*) was
670 downregulated.

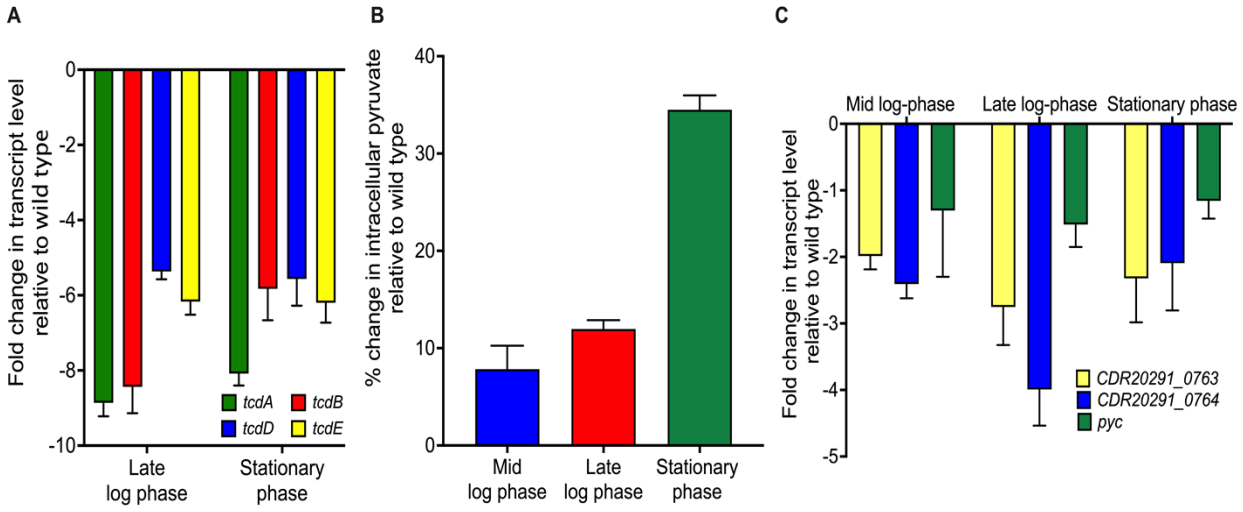

671

672 **Figure 6. Relationship between *tcdA* expression and pyruvate accumulation in cells. A.** RT-
673 qPCR confirmed the downregulation of *tcdA*, *tcdB*, *tcdD* and *tcdE*, in R20291Δ*feoB1* late-
674 logarithmic (OD600nm=0.6) and stationary phase cultures (OD600nm=0.9). **B.** Pyruvate
675 accumulation was determined and shown to be higher in R20291Δ*feoB1* across the three growth
676 phases. Intracellular concentrations of pyruvate in R20291 at each growth phase were: 1.16 ± 0.13
677 nm, 1.39 ± 0.08 nm and 1.66 ± 0.11 nm, respectively; intracellular concentrations of pyruvate in
678 R20291Δ*feoB1* at each growth phase were 1.25 ± 0.14 nm, 1.55 ± 0.11 nm and 2.24 ± 0.16 nm. **C.**
679 Downregulation of genes encoding enzymes of the oxidative branch of the Krebs cycle of *C.*
680 *difficile*. This is consistent with reduced metabolism of pyruvate via that pathway; *pyc* encodes
681 Pyruvate carboxylase; *CDR20291_0763* aconitase; and *CDR20291_0764* encodes Isocitrate/3-
682 isopropylmalate dehydrogenase.

683

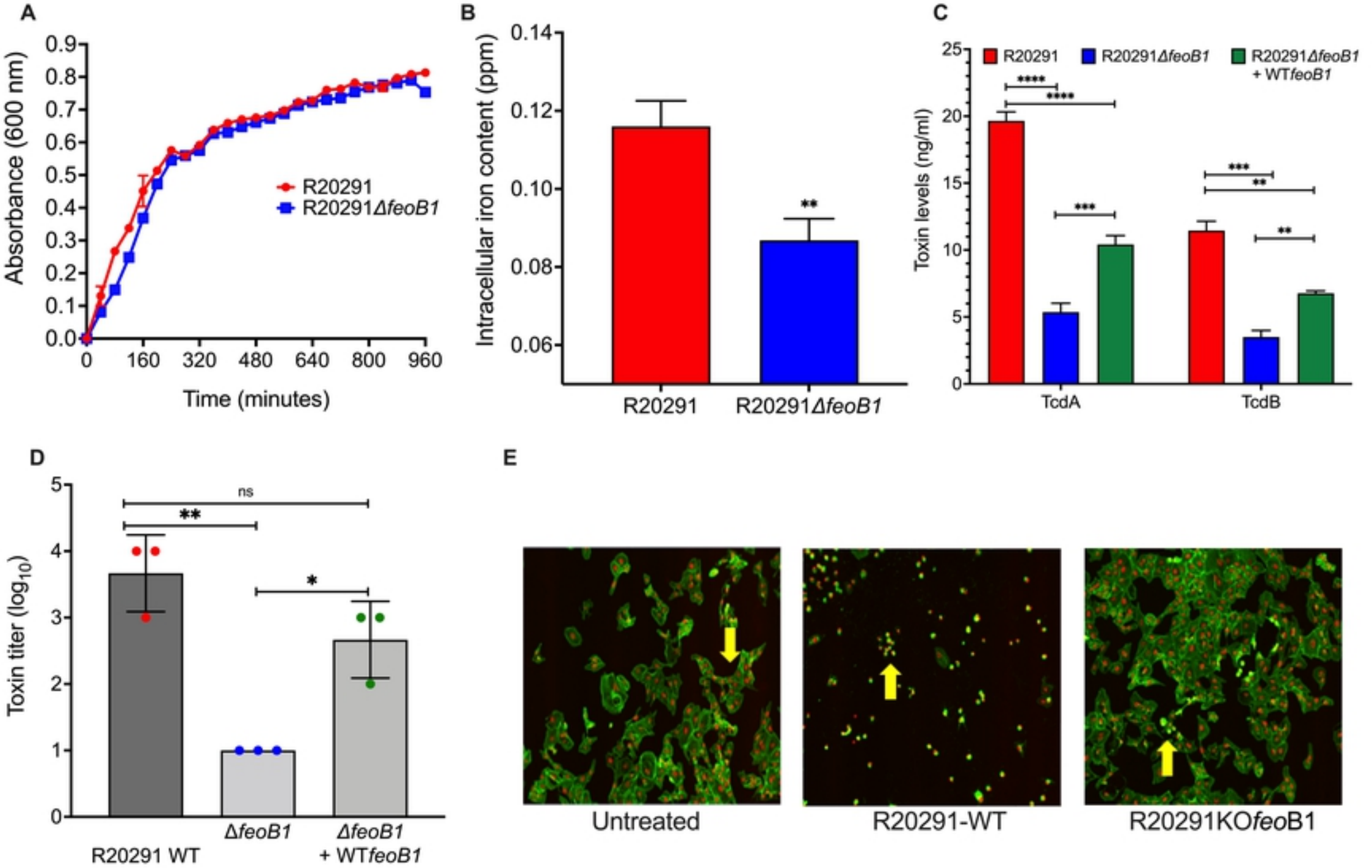
A
Absorbance (600 nm)
Time (minutes)
R20291
R20291ΔfeoB1
B
Intracellular iron content (ppm)
R20291
R20291ΔfeoB1
C
Toxin levels (ng/ml)
R20291
R20291ΔfeoB1
R20291ΔfeoB1 + WTfeoB1
TcdA
TcdB
D
Toxin titer (log10)
ns
R20291 WT
ΔfeoB1
ΔfeoB1 + WTfeoB1
E
Untreated
R20291-WT
R20291KOfeoB1

Figure 1

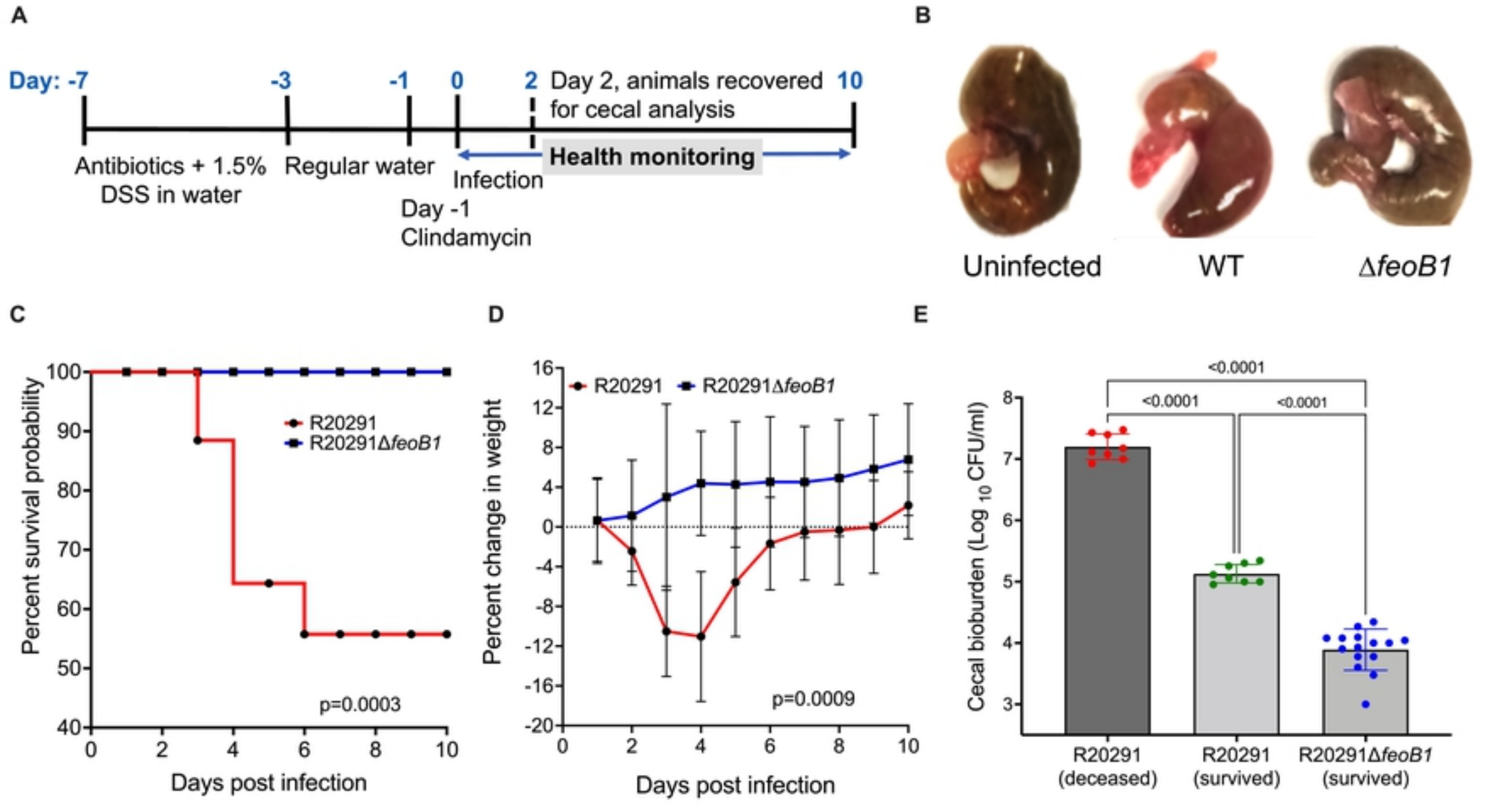
A
Day: -7
-3
-1
0
2
Day 2, animals recovered for cecal analysis
10
Antibiotics + 1.5% DSS in water
Regular water
Infection
Day -1 Clindamycin
Health monitoring
B
Uninfected
WT
ΔfeoB1
C
Percent survival probability
R20291
R20291ΔfeoB1
p=0.0003
Days post infection
D
Percent change in weight
R20291
R20291ΔfeoB1
p=0.0009
Days post infection
E
Cecal bioburden (Log 10 CFU/ml)
<0.0001
<0.0001
<0.0001
R20291 (deceased)
R20291 (survived)
R20291ΔfeoB1 (survived)

Figure 2

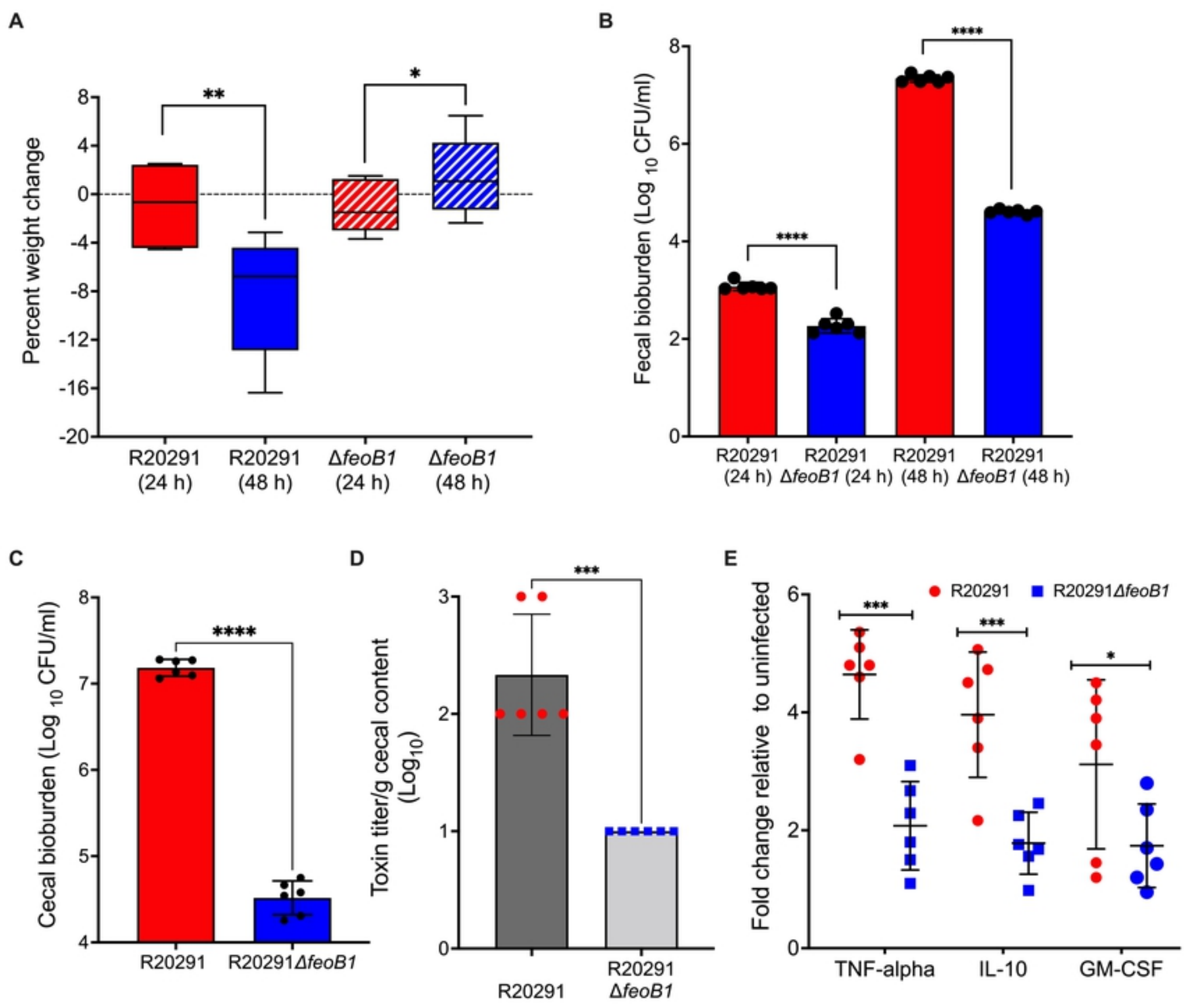
A
Percent weight change
8
4
0
-4
-8
-12
-16
-20
**
*
R20291 (24 h)
R20291 (48 h)
ΔfeoB1 (24 h)
ΔfeoB1 (48 h)
B
Fecal bioburden (Log 10 CFU/ml)
8
6
4
2
0
****
****
R20291 (24 h)
R20291 ΔfeoB1 (24 h)
R20291 (48 h)
R20291 ΔfeoB1 (48 h)
C
Cecal bioburden (Log 10 CFU/ml)
8
7
6
5
4
****
R20291
R20291ΔfeoB1
D
Toxin titer/g cecal content (Log10)
3
2
1
0
***
R20291
R20291 ΔfeoB1
E
Fold change relative to uninfected
6
4
2
0
R20291
R20291ΔfeoB1
***
***
*
TNF-alpha
IL-10
GM-CSF

Figure 3

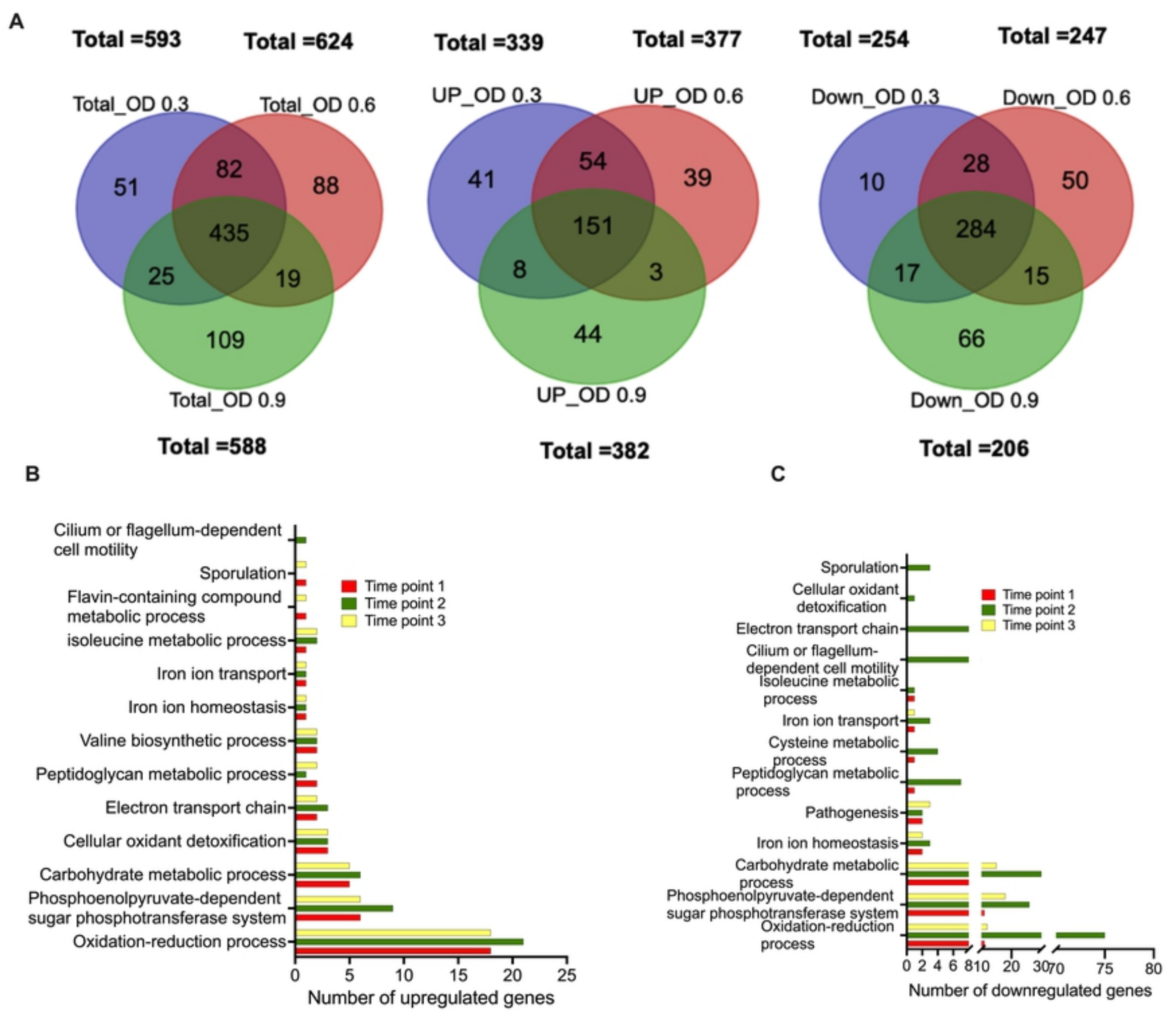
A
Total =593
Total =624
Total =339
Total =377
Total =254
Total =247
Total_OD 0.3
Total_OD 0.6
Total_OD 0.9
51
82
88
435
25
19
109
UP_OD 0.3
UP_OD 0.6
UP_OD 0.9
41
54
39
151
8
3
44
Down_OD 0.3
Down_OD 0.6
Down_OD 0.9
10
28
50
284
17
15
66
Total =588
Total =382
Total =206
B
Cilium or flagellum-dependent cell motility
Sporulation
Flavin-containing compound metabolic process
isoleucine metabolic process
Iron ion transport
Iron ion homeostasis
Valine biosynthetic process
Peptidoglycan metabolic process
Electron transport chain
Cellular oxidant detoxification
Carbohydrate metabolic process
Phosphoenolpyruvate-dependent sugar phosphotransferase system
Oxidation-reduction process
Time point 1
Time point 2
Time point 3
0
5
10
15
20
25
Number of upregulated genes
C
Sporulation
Cellular oxidant detoxification
Electron transport chain
Cilium or flagellum-dependent cell motility
Isoleucine metabolic process
Iron ion transport
Cysteine metabolic process
Peptidoglycan metabolic process
Pathogenesis
Iron ion homeostasis
Carbohydrate metabolic process
Phosphoenolpyruvate-dependent sugar phosphotransferase system
Oxidation-reduction process
Time point 1
Time point 2
Time point 3
0 2 4 6 8 10 20 30 70 75 80
Number of downregulated genes

Figure 4

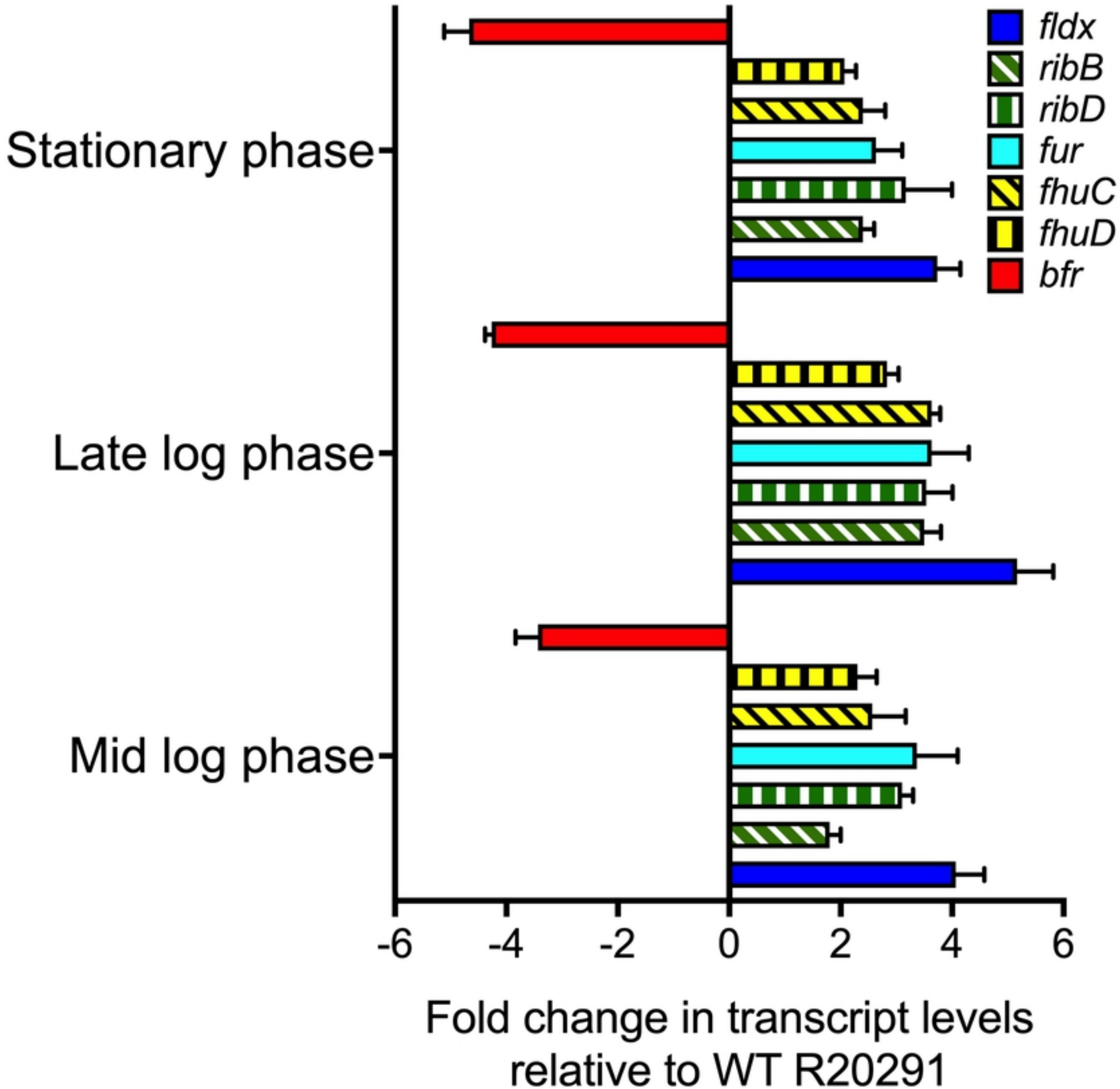
fldx
ribB
ribD
fur
fhuC
fhuD
bfr
Stationary phase
Late log phase
Mid log phase
-6
-4
-2
0
2
4
6
Fold change in transcript levels
relative to WT R20291

Figure 5

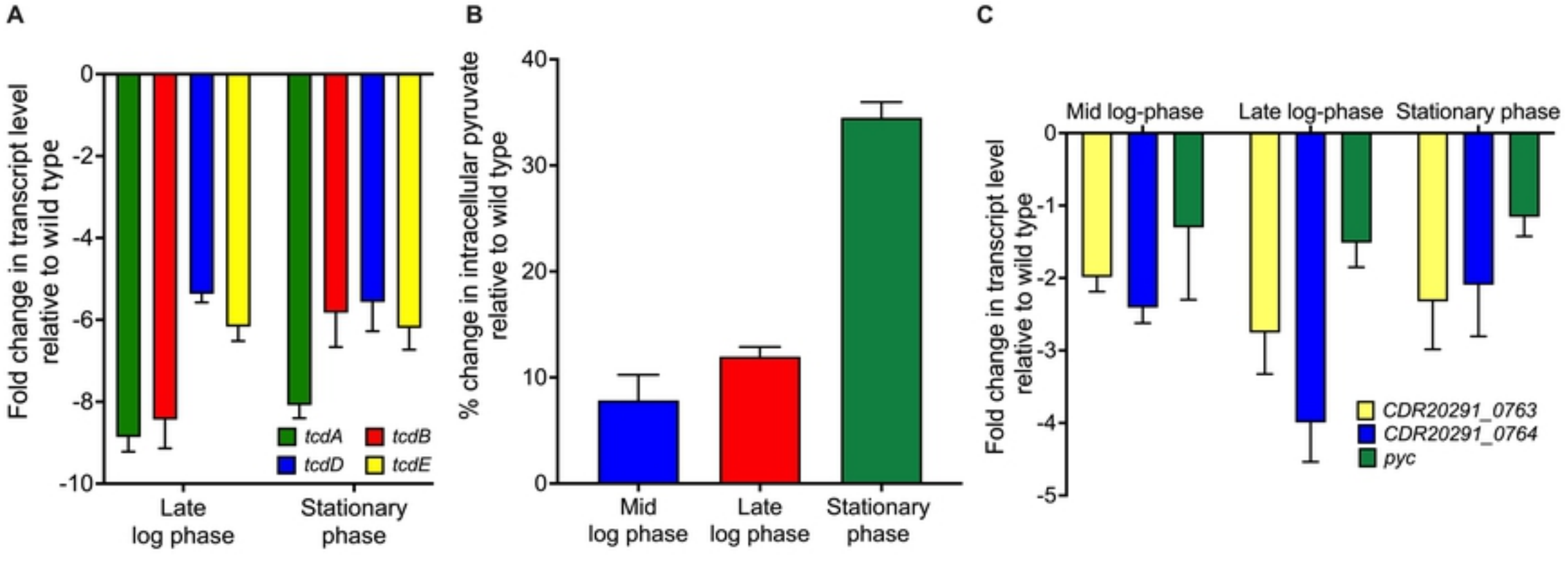
A
Fold change in transcript level relative to wild type
0
-2
-4
-6
-8
-10
tcdA
tcdB
tcdD
tcdE
Late log phase
Stationary phase
B
% change in intracellular pyruvate relative to wild type
40
30
20
10
0
Mid log phase
Late log phase
Stationary phase
C
Mid log-phase
Late log-phase
Stationary phase
Fold change in transcript level relative to wild type
0
-1
-2
-3
-4
-5
CDR20291_0763
CDR20291_0764
pyc

Figure 6